



Spin dynamics during chirped pulses: applications to homonuclear decoupling and broadband excitation

Mohammadali Foroozandeh

Chemistry Research Laboratory, University of Oxford, Mansfield Road, Oxford OX1 3TA, UK



ARTICLE INFO

Article history:

Received 11 April 2020

Revised 27 May 2020

Accepted 2 June 2020

Keywords:

Chirped pulses
Liouville-von Neumann equation
Wei-Norman Lie algebra
Differential equations
Homonuclear decoupling
PSYCHE
Broadband excitation
CHORUS

ABSTRACT

Swept-frequency pulses have found applications in a wide range of areas including spectroscopic techniques where efficient control of spins is required. For many of these applications, a good understanding of the evolution of spin systems during these pulses plays a vital role, not only in describing the mechanism of techniques, but also in enabling new methodologies. In magnetic resonance spectroscopy, broadband inversion, refocusing, and excitation using these pulses are among the most used applications in NMR, ESR, MRI, and *in vivo* MRS. In the present survey, a general expression for chirped pulses will be introduced, and some numerical approaches to calculate the spin dynamics during chirped pulses via solutions of the well-known Liouville-von Neumann equation and the lesser-explored Wei-Norman Lie algebra along with comprehensive examples are presented. In both cases, spin state trajectories are calculated using the solution of differential equations. Additionally, applications of the proposed methods to study the spin dynamics during the PSYCHE pulse element for broadband homonuclear decoupling and the CHORUS sequence for broadband excitation will be presented.

© 2020 Elsevier Inc. All rights reserved.

1. Introduction

Swept-frequency pulses are a group of parametric pulses during which the frequency of irradiation varies with time. They are generally called according to the distribution function of their frequency sweep, e.g. linear (chirped pulses), hyperbolic secant (HS pulses), hyperbolic tangent (Tanh pulses), etc. In particular, the ability of swept-frequency pulses to satisfy adiabatic condition [1] under certain circumstances is very attractive in many applications [2–5]. The adiabatic properties of swept-frequency pulses cause that sometimes, misleadingly, these pulses are called "adiabatic pulses" even when they do not satisfy the adiabatic condition. In two examples presented in this paper, chirped pulses are used partially or totally below the adiabatic threshold.

Swept-frequency pulses have found a surprisingly wide range of applications in magnetic resonance, including but not limited to, designing robust broadband inversion and refocusing [6–21] and excitation [22–31] pulses, designing B_1 -insensitive pulses [32–34,14,35–39], broadband heteronuclear decoupling [40–46,16,47–49], single scan NMR [50,51], spatiotemporal encoding [52–54], solid-state NMR [8,55,20,56–58], dynamic nuclear polarization (DNP) [59–62], coherence suppression [63–65], broadband electron spin resonance (ESR) [66,67,21,68–83], and designing cpmg sequences [84–87].

Additionally they have found applications in adiabatic optimal control for logic gate design for quantum computing [88–95], and manipulation of NV-centers in diamond [96–99].

In many of these applications, understanding of the spin dynamics during the pulse event is as important as knowing the state of the system at the end of the pulse event. This is particularly important when some trajectories for certain coherences should be enforced or suppressed. The aim of the present article is to set a unified approach for the calculation and visualisation of the spin dynamics during chirped pulses and pulse sequences consisting only of chirped pulses using the solution of a single system of ordinary differential equations (ODEs). The proposed scheme will be presented in the context of two different mathematical formalisms: the first gives access to the solution of familiar Liouville-von Neumann equation, and the second takes advantage of Wei-Norman Lie algebra, a powerful, but rarely explored technique in magnetic resonance.

The motivation behind this proposition is threefold: (i) As opposed to the conventional density matrix approach, relying on matrix exponentiation and piecewise constant propagation, ODE integrators have an adaptive time-step selection which changes depends on the local frequency of the oscillation. This property enables much faster computation of the spin dynamics during swept-frequency pulses, with fewer time steps for the same accuracy. This feature is especially attractive when computation of the spin dynamics during swept-frequency pulses is part of an iterative

E-mail address: mohammadali.foroozandeh@chem.ox.ac.uk

process like optimisation. (ii) Although the conventional density matrix approach could be more general, as it can, in principle, handle sudden changes and discontinuities in the Hamiltonian, swept-frequency pulses are smooth, time-continuous by nature, ideal for adaptive non-stiff ODE integrators (e.g. ode45 in MATLAB). (iii) both proposed approaches based on Liouville-von Neumann equation and Wei-Norman Lie algebra can lead to analytical or closed-form solutions and hold promise for more efficient construction and optimisation of pulse sequences consisting of swept frequency pulses.

This paper is structured as follows: in Section 2 a general expression for swept-frequency (chirped pulses in particular) will be introduced, followed by detailed presentations of Liouville-von Neumann equation and Wei-Norman Lie algebra. For both approaches, general mathematical formalisms are presented, along with examples representing the applications of these formalisms in cases relevant to NMR. Finally, each method has a "demo" NMR technique, demonstrating how the proposed approach gives access to the desired information about the spin dynamics. In Section 3 a comprehensive usage of the proposed approaches will be presented for broadband homonuclear decoupling using a PSYCHE pulse element and broadband chirped excitation using a CHORUS pulse sequence.

2. Theory

Remark 1. All solutions presented in this article are numeric, obtained using the adaptive Runge–Kutta method [100]. Similar results can be obtained using other proposed methods relying on the approximation of matrix exponentials and Fokker–Planck formalism [101,102], available via SPINACH package [103]. Approximated analytical solutions can be obtained using instantaneous flip approximation during chirped pulses [54]. Exact and explicit closed-form or analytical solutions can be obtained using various techniques, including the application of integrable systems [104,105] and algebraic graph theory [106]. These solutions, even for coupled spins, can be represented as analytical or closed-form expressions using transcendental functions (hypergeometric, Whittaker, Fresnel integrals, etc.) and will be presented elsewhere. Although, some analytical solutions of the Bloch equations for swept-frequency pulses, in particular hyperbolic secant pulses, have been presented in the literature [107,108].

2.1. Generalised chirped pulse

It is typical to write the general form of swept-frequency pulses as:

$$S(t) = \omega_1(t) \exp(i\phi(t)) \quad (1)$$

where the amplitude envelope $\omega_1(t)$ and the phase $\phi(t)$ are continuous, real-valued functions of time. The relationship between frequency sweep function $\omega(t)$ and phase $\phi(t)$ of the pulse can be written as:

$$\phi(t) = \int_0^{\tau_p} \omega(t) dt \quad (2)$$

Although in the rest of this paper only chirped pulses with a linear frequency sweep, and therefore a quadratic phase, are considered, the framework is general and can be applied to any form of parametrised pulses with time-continuous parameters.

We start with the introduction of the most general form of a chirped pulse. As opposed to the conventional 3-parameter chirp pulse described by amplitude (ω_1), duration (τ_p), and bandwidth (ΔF), these pulses are described by 6 parameters: amplitude (ω_1), bandwidth (ΔF), duration (τ_p), overall phase (ϕ_0), time offset (δ_t),

and frequency offset (δ_f). These additional parameterisations, as will be shown later, allow us to construct any type of pulse sequence consisting of chirped pulses, either concatenated or superimposed, very easily as a single sum of time-continuous functions. Additionally, any further offset modulation or overall phase variation (as in phase cycling) can be incorporated in this expression.

Most commonly, smoothing of the time-envelope for chirped pulses is achieved via the application of WURST [43], or quarter-sine [109] smoothing functions. For a generalised chirped pulse, presented here, the time-envelope is a super-Gaussian distribution, covering the whole sequence:

$$G(t) = \exp \left[-2^{n+2} \left(\frac{t - \delta_t}{\tau_p} \right)^n \right], \quad n \in 2\mathbb{Z}^+ \quad (3)$$

Here δ_t and τ_p are related to the mean and variance of the distribution respectively, and n is an even number determining the smoothing of the time envelope, where for $n = 2$ a normal Gaussian envelope will be obtained. Generally n in the range of 20 to 40 will be adequate for most applications.

The complete expression for a generalised chirped pulse can be written as:

$$S(t) = \omega_1 \times \exp \left[-2^{n+2} \left(\frac{t - \delta_t}{\tau_p} \right)^n + i \left(\phi_0 + \frac{\pi \Delta F (t - \delta_t)^2}{\tau_p} - 2\pi \delta_f (t - \delta_t) \right) \right] \quad (4)$$

Eq. (4) can also be represented in Cartesian coordinates as:

$$S(t) = C_x(t) + iC_y(t) \quad (5)$$

where

$$C_x(t) = \omega_1 \exp \left[-2^{n+2} \left(\frac{t - \delta_t}{\tau_p} \right)^n \right] \cos \left[\phi_0 + \frac{\pi \Delta F (t - \delta_t)^2}{\tau_p} - 2\pi \delta_f (t - \delta_t) \right] \quad (6)$$

and

$$C_y(t) = \omega_1 \exp \left[-2^{n+2} \left(\frac{t - \delta_t}{\tau_p} \right)^n \right] \sin \left[\phi_0 + \frac{\pi \Delta F (t - \delta_t)^2}{\tau_p} - 2\pi \delta_f (t - \delta_t) \right] \quad (7)$$

Fig. 1 shows a complex chirped pulse with its real ($C_x(t)$) and imaginary ($C_y(t)$) components.

Eqs. (4), (6) and (7) can be used to construct any pulse sequence consisting of chirped pulses as a sum of generalised chirped pulses:

$$S(t) = \sum_{i=1}^I \omega_1^{(i)} \times \exp \left[-2^{n+2} \left(\frac{t - \delta_t^{(i)}}{\tau_p^{(i)}} \right)^n + i \left(\phi_0^{(i)} + \frac{\pi \Delta F (t - \delta_t^{(i)})^2}{\tau_p^{(i)}} - 2\pi \delta_f^{(i)} (t - \delta_t^{(i)}) \right) \right] \quad (8)$$

where I is the number of chirped pulses. Note that due to the nature of super-Gaussian time envelopes, there is no need for explicit inclusion of delays in the sequence and those can be incorporated using an appropriate time offset δ_t of each pulse. Again the Cartesian components of $S(t)$ are:

$$C_x(t) = \sum_{i=1}^I \omega_1^{(i)} \exp \left[-2^{n+2} \left(\frac{t - \delta_t^{(i)}}{\tau_p^{(i)}} \right)^n \right] \cos \left[\phi_0^{(i)} + \frac{\pi \Delta F (t - \delta_t^{(i)})^2}{\tau_p^{(i)}} - 2\pi \delta_f^{(i)} (t - \delta_t^{(i)}) \right] \quad (9)$$

and

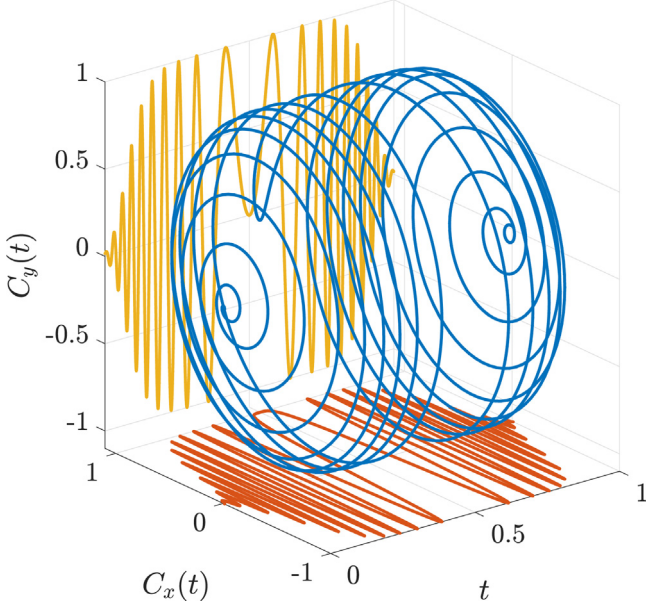


Fig. 1. Graphical representation of a complex chirped pulse as presented in Eq. (4), and its orthogonal components, $C_x(t)$ and $C_y(t)$, for a pulse with $\Delta F = 60$ kHz, $\tau_p = 1$ ms, $\delta_t = 0.5$ ms, $\phi_0 = 0$, $\delta_f = 0$, $\omega_1 = 1$, and $n = 10$.

$$C_y(t) = \sum_{i=1}^l \omega_1^{(i)} \exp \left[-2^{n+2} \left(\frac{t - \delta_t^{(i)}}{\tau_p^{(i)}} \right)^n \right] \sin \left[\phi_0^{(i)} + \frac{\pi \Delta F (t - \delta_t^{(i)})^2}{\tau_p^{(i)}} - 2\pi \delta_f^{(i)} (t - \delta_t^{(i)}) \right] \quad (10)$$

Fig. 2 shows the effect of super-Gaussian smoothing and additional parametrisation on a chirped waveform.

As will be demonstrated in Section 3.2, the proposed general scheme for defining chirped pulses is not only useful for the generation and description of chirped pulse sequences, but also when certain optimisation approaches take advantage of parametrised, or semi-parametrised waveforms [110,111].

2.2. Liouville-von Neumann equation

In this section we consider construction of a matrix homogeneous ODE (ordinary differential equation) to have access to time-dependent evolution of each member of the basis set \mathcal{L} . Explicit examples will be provided in the succeeding sections, but first let us consider the most general case. For a basis set $\mathcal{L} = \{X_1, X_2, \dots, X_N\}$, we consider that the set is closed under all possible pair-wise commutations, i.e.

$$[X_i, X_j] = \lambda_{ij} X_k, \quad \lambda_{ij} \in \mathbb{C}, \quad X_k \in \mathcal{L} \quad (11)$$

The Hamiltonian of the system can be written as a finite sum of elements of the basis set with corresponding coefficients (γ) that could be constant or time-dependent.

$$\mathcal{H}(t) = \sum_{i=1}^N \gamma_i(t) X_i \quad (12)$$

Note that this is a general construction and some coefficients, γ , could be 0.

We are interested in the time evolution of individual elements of the basis set \mathcal{L} , the solution of which is given by the Liouville-von Neumann equation for the time evolution of the density matrix of the system, $\rho(t)$:

$$\frac{\partial \rho(t)}{\partial t} = -i[\mathcal{H}(t), \rho(t)] \quad (13)$$

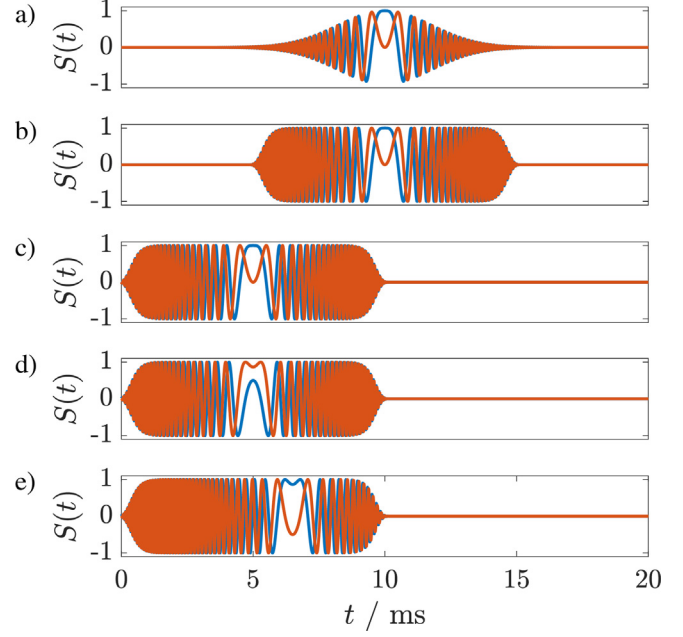


Fig. 2. Graphical representation of Cartesian components ($C_x(t)$ in blue and $C_y(t)$ in red) of a chirped pulse with $\Delta F = 20$ kHz, $\tau_p = 10$ ms, and $\omega_1 = 1$ in a time frame of 20 ms; a) with $\phi_0 = 0$, $\delta_t = 10$ ms, $\delta_f = 0$, and $n = 2$, b) the same as (a) but with $n = 10$, c) the same as (b) but with $\delta_t = 5$ ms, d) the same as (c) but with $\phi_0 = \frac{\pi}{3}$, and e) the same as (d) but with $\delta_f = 3000$ Hz.

Similar to the Hamiltonian, we write the density matrix as a finite sum of elements of the basis set \mathcal{L} and their time-dependent coefficients:

$$\rho(t) = \sum_{j=1}^N g_j(t) X_j \quad (14)$$

by replacing Eqs. (12) and (14) in Eq. (13) we have:

$$\sum_{j=1}^N \dot{g}_j(t) X_j = -i \left[\sum_{i=1}^N \gamma_i X_i, \sum_{j=1}^N g_j(t) X_j \right] = -i \sum_{i=1}^N \sum_{j=1}^N \gamma_i g_j(t) [X_i, X_j] \quad (15)$$

This equation can be written in vector and matrix form as

$$\mathcal{L}\dot{\mathbf{g}}(t) = -i\gamma \mathbf{X}_{[:,]} \mathbf{g}(t) \quad (16)$$

where

$$\gamma = [\gamma_1, \gamma_2, \dots, \gamma_N] \quad (17)$$

$$\mathbf{X}_{[:,]} = \begin{pmatrix} [X_1, X_1] & [X_1, X_2] & \cdots & [X_1, X_N] \\ [X_2, X_1] & [X_2, X_2] & \cdots & [X_2, X_N] \\ \vdots & \vdots & \ddots & \vdots \\ [X_N, X_1] & [X_N, X_2] & \cdots & [X_N, X_N] \end{pmatrix} \quad (18)$$

and

$$\mathbf{g}(t) = [g_1(t), g_2(t), \dots, g_N(t)]^T \quad (19)$$

with $\dot{\mathbf{g}}(t)$ being time derivative of $\mathbf{g}(t)$.

By collecting and ordering coefficients of the basis set $\mathcal{L} = \{X_1, X_2, \dots, X_N\}$ we can re-write the Eq. (16) as

$$\mathcal{L}\dot{\mathbf{g}}(t) = -i\mathcal{L}\Gamma\mathbf{g}(t) \quad (20)$$

and therefore

$$\dot{\mathbf{g}}(t) = -i\Gamma\mathbf{g}(t) \quad (21)$$

where Γ is a matrix of the Hamiltonian coefficients, elements of which can be obtained as:

$$\Gamma_{mn} = \sum_{i=1}^N \gamma_i \lambda_{in} \quad (22)$$

when for each pair X_i and X_n , $[X_i, X_n] = \lambda_{in} X_m$.

2.2.1. Example: single spin- $\frac{1}{2}$

For a single spin- $\frac{1}{2}$ the basis set can be written using ladder operators of Pauli matrices (σ_α , $\alpha \in \{x, y, z\}$):

$$\mathcal{L} = \{\sigma^-, \sqrt{2}\sigma_z, \sigma^+\} \quad (23)$$

where $\sigma^- = \sigma_x - i\sigma_y$ and $\sigma^+ = \sigma_x + i\sigma_y$.

Remark 2. The unitary operator is discarded from the basis set \mathcal{L} for simplicity, although its inclusion will not change the mathematical approach, neither the results, presented in this article.

In the presence of a chirped pulse as in Eq. (4) with \mathcal{RF} amplitude (ω_1), bandwidth (ΔF), duration (τ_p), overall phase (ϕ_0), time offset (δ_t), and frequency offset (δ_f), the Hamiltonian can be written as:

$$\mathcal{H}(t) = \beta\sigma^- + \beta^*\sigma^+ + \Omega\sigma_z \quad (24)$$

where Ω is the spin resonance offset,

$$\begin{aligned} \beta &= \frac{1}{2}\omega_1 \\ &\times \exp \left[-2^{n+2} \left(\frac{t - \delta_t}{\tau_p} \right)^n + i \left(\phi_0 + \frac{\pi\Delta F(t - \delta_t)^2}{\tau_p} - 2\pi\delta_f(t - \delta_t) \right) \right] \end{aligned} \quad (25)$$

and * indicates complex conjugate.

The array of Hamiltonian coefficients can be written as:

$$\gamma = \left[\beta, \frac{\Omega}{\sqrt{2}}, \beta^* \right] \quad (26)$$

and according to Eq. (18) for the basis set shown in Eq. (23) we have

$$\begin{aligned} \mathbf{X}_{[.,.]} &= \begin{pmatrix} [\sigma^-, \sigma^-][\sigma^-, \sqrt{2}\sigma_z] & [\sigma^-, \sigma^+] \\ [\sqrt{2}\sigma_z, \sigma^-] & [\sqrt{2}\sigma_z, \sqrt{2}\sigma_z] & [\sqrt{2}\sigma_z, \sigma^+] \\ [\sigma^+, \sigma^-][\sigma^+, \sqrt{2}\sigma_z] & [\sigma^+, \sigma^+] \end{pmatrix} \\ &= \begin{pmatrix} 0 & \sqrt{2}\sigma^- & -2\sigma_z \\ -\sqrt{2}\sigma^- & 0 & \sqrt{2}\sigma^+ \\ 2\sigma_z & -\sqrt{2}\sigma^+ & 0 \end{pmatrix} \end{aligned} \quad (27)$$

$$\begin{aligned} i \begin{pmatrix} \dot{g}_1(t) \\ \dot{g}_2(t) \\ \dot{g}_3(t) \\ \dot{g}_4(t) \\ \dot{g}_5(t) \\ \dot{g}_6(t) \\ \dot{g}_7(t) \\ \dot{g}_8(t) \\ \dot{g}_9(t) \\ \dot{g}_{10}(t) \\ \dot{g}_{11}(t) \\ \dot{g}_{12}(t) \\ \dot{g}_{13}(t) \\ \dot{g}_{14}(t) \\ \dot{g}_{15}(t) \end{pmatrix} &= \begin{pmatrix} 0 & 0 & \mathcal{J} & -\mathcal{J} & 0 & \mathcal{B} & -\mathcal{B}^* & 0 & 0 & 0 & 0 & 0 & 0 & 0 & 0 & 0 \\ 0 & 0 & -\mathcal{J} & \mathcal{J} & 0 & 0 & 0 & \mathcal{B} & -\mathcal{B}^* & 0 & 0 & 0 & 0 & 0 & 0 & 0 \\ \mathcal{J} & -\mathcal{J} & -\Delta & 0 & 0 & 0 & 0 & 0 & 0 & -\mathcal{B} & 0 & 0 & \mathcal{B}^* & 0 & 0 & 0 \\ -\mathcal{J} & \mathcal{J} & 0 & \Delta & 0 & 0 & 0 & 0 & 0 & 0 & \mathcal{B}^* & -\mathcal{B} & 0 & 0 & 0 & 0 \\ 0 & 0 & 0 & 0 & 0 & 0 & 0 & 0 & 0 & \mathcal{B} & -\mathcal{B}^* & \mathcal{B} & -\mathcal{B}^* & 0 & 0 & 0 \\ \mathcal{B}^* & 0 & 0 & 0 & 0 & -\Omega_1 & 0 & 0 & 0 & -\mathcal{J} & 0 & \mathcal{J} & 0 & 0 & 0 & 0 \\ \dot{g}_7(t) & -\mathcal{B} & 0 & 0 & 0 & 0 & \Omega_1 & 0 & 0 & 0 & \mathcal{J} & 0 & -\mathcal{J} & 0 & 0 & 0 \\ \dot{g}_8(t) & 0 & \mathcal{B}^* & 0 & 0 & 0 & 0 & 0 & -\Omega_2 & 0 & \mathcal{J} & 0 & -\mathcal{J} & 0 & 0 & 0 \\ \dot{g}_9(t) & 0 & -\mathcal{B} & 0 & 0 & 0 & 0 & 0 & \Omega_2 & 0 & 0 & -\mathcal{J} & 0 & \mathcal{J} & 0 & 0 \\ \dot{g}_{10}(t) & 0 & 0 & -\mathcal{B}^* & 0 & \mathcal{B}^* & -\mathcal{J} & 0 & \mathcal{J} & 0 & -\Omega_1 & 0 & 0 & 0 & \mathcal{B} & 0 \\ \dot{g}_{11}(t) & 0 & 0 & 0 & \mathcal{B} & -\mathcal{B} & 0 & \mathcal{J} & 0 & -\mathcal{J} & 0 & \Omega_1 & 0 & 0 & 0 & -\mathcal{B}^* \\ \dot{g}_{12}(t) & 0 & 0 & 0 & -\mathcal{B}^* & \mathcal{B}^* & \mathcal{J} & 0 & -\mathcal{J} & 0 & 0 & 0 & -\Omega_2 & 0 & \mathcal{B} & 0 \\ \dot{g}_{13}(t) & 0 & 0 & \mathcal{B} & 0 & -\mathcal{B} & 0 & -\mathcal{J} & 0 & \mathcal{J} & 0 & 0 & 0 & \Omega_2 & 0 & -\mathcal{B}^* \\ \dot{g}_{14}(t) & 0 & 0 & 0 & 0 & 0 & 0 & 0 & 0 & 0 & \mathcal{B}^* & 0 & \mathcal{B}^* & 0 & -\Sigma & 0 \\ \dot{g}_{15}(t) & 0 & 0 & 0 & 0 & 0 & 0 & 0 & 0 & 0 & 0 & -\mathcal{B} & 0 & -\mathcal{B} & 0 & \Sigma \end{pmatrix} \begin{pmatrix} g_1(t) \\ g_2(t) \\ g_3(t) \\ g_4(t) \\ g_5(t) \\ g_6(t) \\ g_7(t) \\ g_8(t) \\ g_9(t) \\ g_{10}(t) \\ g_{11}(t) \\ g_{12}(t) \\ g_{13}(t) \\ g_{14}(t) \\ g_{15}(t) \end{pmatrix} \end{aligned} \quad (34)$$

Therefore, Eq. (21) for this system can be written as:

$$\begin{pmatrix} \dot{g}_1(t) \\ \dot{g}_2(t) \\ \dot{g}_3(t) \end{pmatrix} = -i \begin{pmatrix} -\Omega & \sqrt{2}\beta & 0 \\ \sqrt{2}\beta^* & 0 & -\sqrt{2}\beta \\ 0 & -\sqrt{2}\beta^* & \Omega \end{pmatrix} \begin{pmatrix} g_1(t) \\ g_2(t) \\ g_3(t) \end{pmatrix} \quad (28)$$

2.2.2. Example: Two-spin- $\frac{1}{2}$ system with scalar coupling

For a two-spin- $\frac{1}{2}$ system the basis set contains 15 orthonormal terms. Again, the choice of basis set and the order of elements in the basis set is user-defined. For the following demonstration we consider the basis set as follows:

By considering

$$P_\alpha = \sigma_\alpha \otimes \mathbb{1}, \quad Q_\alpha = \mathbb{1} \otimes \sigma_\alpha, \quad \alpha \in \{x, y, z\} \quad (29)$$

and

$$P^\pm = P_x \pm iP_y, \quad Q^\pm = Q_x \pm iQ_y \quad (30)$$

we can write the basis set consisting of all 15 terms, including 5 zero quantum, 8 single quantum, and 2 double quantum terms.

$$\begin{aligned} \mathcal{L} = \{ &P_z, Q_z, P^-Q^+, P^+Q^-, 2P_zQ_z, \\ &\frac{P^-}{\sqrt{2}}, \frac{P^+}{\sqrt{2}}, \frac{Q^-}{\sqrt{2}}, \frac{Q^+}{\sqrt{2}}, \sqrt{2}P^-Q_z, \\ &\sqrt{2}P^+Q_z, \sqrt{2}P_zQ^-, \sqrt{2}P_zQ^+, \\ &P^-Q^-, P^+Q^+ \} \end{aligned} \quad (31)$$

The Hamiltonian for this system under a chirped pulse with a set of parameters specified in the previous section can be written as:

$$\begin{aligned} \mathcal{H}(t) = & \Omega_P P_z + \Omega_Q Q_z + \pi J(P^-Q^+ + P^+Q^- + 2P_zQ_z) \\ & + \beta(P^- + Q^-) + \beta^*(P^+ + Q^+) \end{aligned} \quad (32)$$

According to Eqs. (31) and (32) the coefficient array, γ , can be written as:

$$\gamma = [\Omega_P, \Omega_Q, \pi J, \pi J, \pi J, \sqrt{2}\beta, \sqrt{2}\beta^*, \sqrt{2}\beta, \sqrt{2}\beta^*, 0, 0, 0, 0, 0, 0] \quad (33)$$

After constructing $\mathbf{X}_{[.,.]}$ Eq. (18) using all pairwise commutations of the basis set \mathcal{L} for this system, the homogeneous ODE of Eq. (21) for the time coefficients of the basis set can be written as Eq. (34), where

$$\mathcal{J} = \pi J, \quad \mathcal{B} = \sqrt{2}\beta, \quad \Sigma = \Omega_P + \Omega_Q, \quad \Delta = \Omega_P - \Omega_Q$$

2.2.3. Demo: Zero-quantum suppression

The elegant idea of the suppression of zero quantum coherences using spatiotemporal averaging was first introduced by Thrippleton and Keeler [64]. Here the general attenuation mechanism of this method on a two-spin- $\frac{1}{2}$ system is presented. The pulse element simply consists of a 180° chirped pulse applied simultaneously with a pulsed field gradient. The maximum \mathcal{RF} amplitude of a chirped pulse can be calculated as:

$$\mathcal{RF}_{max} = \sqrt{\frac{\Delta F Q}{2\pi\tau_p}} \quad (35)$$

where Q is the adiabaticity factor. The relationship between Q factor and pulse flip angle α can be written as [70]:

$$Q = \frac{2}{\pi} \ln \left(\frac{2}{\cos(\alpha) + 1} \right) \quad (36)$$

The effective flip angle of a chirped pulse approaches 180° asymptotically as the \mathcal{RF} increases, therefore a value of Q factor (5 for most practical purposes) is chosen as a threshold in order to satisfy the adiabatic condition with an affordable \mathcal{RF} amplitude.

The Hamiltonian for two coupled spins in the presence of a chirped pulse and simultaneous pulsed field gradient can be written as:

$$\begin{aligned} \mathcal{H}(t) = & \Omega_p P_z + \Omega_Q Q_z + \pi J(P^- Q^+ + P^+ Q^- + 2P_z Q_z) \\ & + \beta(P^- + Q^-) + \beta^*(P^+ + Q^+) + \Omega_g(z)(P_z + Q_z) \end{aligned} \quad (37)$$

Since for a single chirped pulse here $\delta_t = 0$, $\delta_f = 0$, and $\phi_0 = 0$:

$$\beta = \frac{1}{2} \omega_1 \exp \left[-2^{n+2} \left(\frac{t - \frac{\tau_p}{2}}{\tau_p} \right)^n + i \left(\frac{\pi \Delta F (t - \frac{\tau_p}{2})^2}{\tau_p} \right) \right] \quad (38)$$

The bandwidth of the frequency distribution induced by the field gradient is

$$\Delta \Omega_g = \gamma_H L G_z, \quad (39)$$

where γ_H is the gyromagnetic ratio of proton and L is the length of the active volume exposed to a pulsed field gradient along z axis (G_z). The frequency offset induced at each part of the active volume can be written as

$$\Omega_g(z) = \gamma_H z G_z, \quad z \in \left[-\frac{L}{2}, \frac{L}{2} \right]. \quad (40)$$

For practical implementation in order to avoid unnecessary signal loss due to diffusion or excessive spatial encoding normally the strength of the gradient G_z is set to a value so that $\Omega_g(z) \in [-\pi \Delta F, +\pi \Delta F]$.

The array of coefficients for this system can be written as:

$$\begin{aligned} \gamma = & [\Omega_p + \Omega_g(z), \Omega_Q + \Omega_g(z), \pi J, \pi J, \\ & \sqrt{2}\beta, \sqrt{2}\beta^*, \sqrt{2}\beta, \sqrt{2}\beta^*, 0, 0, 0, 0, 0, 0] \end{aligned} \quad (41)$$

Now including these in Eq. (34) we can set the ODE for this system. We need to replace Ω_p and Ω_Q with $\Omega_p + \Omega_g(z)$ and $\Omega_Q + \Omega_g(z)$ respectively. Additionally we have:

$$\mathcal{J} = \pi J, \quad \mathcal{B} = \sqrt{2}\beta, \quad \Sigma = \Omega_p + \Omega_Q + 2\Omega_g(z), \quad \Delta = \Omega_p - \Omega_Q$$

In order to gain useful insight about the mechanism of zero quantum suppression using spatiotemporal averaging, let us define a parameter ξ indicating a unique relationship between spin system and pulse element parameters:

$$\xi = \sqrt{\frac{\theta}{\mathcal{R}}} \quad (42)$$

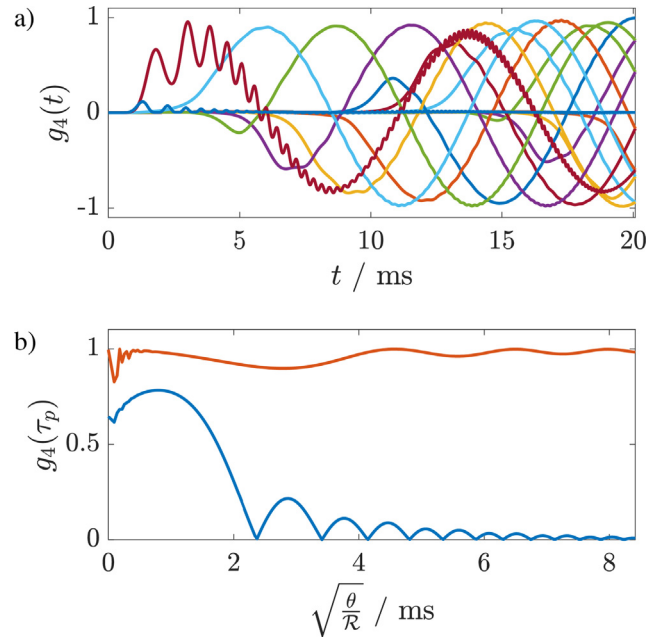


Fig. 3. Graphical representation of zero quantum coherence during a chirped pulse applied simultaneously with a pulsed field gradient; (a) time variation of $g_4(t)$ corresponding to zero quantum term P^+Q^- for 15 different values of $\Omega_g(z)$ during a pulse element with $\tau_p = 20$ ms, $\Delta F = 10000$ Hz, $\Omega_g = 2\pi 10000$, (b) time variation of $g_4(\tau_p)$ as a function of ξ in the absence (red) and presence (blue) of the pulsed field gradient. (For interpretation of the references to colour in this figure legend, the reader is referred to the web version of this article.)

where

$$\theta = \left| \frac{\Delta}{2\pi J} \right|, \quad \mathcal{R} = \frac{\Delta F}{\tau_p}$$

Note that here \mathcal{R} is the sweep-rate of the pulse and θ indicates the strength of the interaction between spins. As the phase of a zero quantum coherence is time dependent, a combination of linear-sweep irradiation of spins with pulsed field gradient induces a time-dependent phase variation of unwanted zero quantum coherences across the sample volume. In order to demonstrate the effect of this pulse element, let us consider that only one zero quantum term P^-Q^+ exists before the pulse element, i.e. $g_3(0) = 1$. As the chirped pulse is 180° we are interested to see how much $g_4(\tau_p)$ corresponding to term P^+Q^- is generated at the end of the pulse element.

Fig. 3(a) shows the variation of $g_4(t)$ during a zero quantum filter at different parts of the sample volume. It is evident that zero quantum signals at different parts of the sample acquire time-dependent phase shift leading of an efficient attenuation of those signals via ensemble averaging. Fig. 3(b) represents the efficiency of the zero quantum attenuation by plotting $g_4(\tau_p)$ as a function of ξ in Eq. (42) in the presence and absence of spatial averaging. The blue graph in Fig. 3(b) suggests that for example for a two-spin system with 200 Hz difference in offsets and 10 Hz J coupling, in order to attenuate the zero-quantum term to 3% with a 10 kHz chirped pulse, the duration of the pulse should be 18 ms.

2.3. Wei-Norman Lie algebra

One elegant way of solving problems presented here was proposed by Wei and Norman [112,113]. Here the goal is to obtain a solution for a time-ordered propagator $\mathcal{U}(t)$ rather than the density

matrix. The solution of the Liouville-von Neumann equation can be written using a time-dependent unitary propagator as:

$$\rho(t) = \mathcal{U}(t)\rho(0)\mathcal{U}(t)^\dagger \quad (43)$$

where $\mathcal{U}(t)$ is the solution of the following differential equation:

$$\frac{d}{dt}\mathcal{U}(t) = -i\mathcal{H}(t)\mathcal{U}(t), \quad \mathcal{U}(0) = 1 \quad (44)$$

with the solution

$$\mathcal{U}(t) = \mathcal{T} \exp \left[-i \int_0^t \mathcal{H}(t') dt' \right] \quad (45)$$

where \mathcal{T} is the time-ordering operator. The goal is, relying on the Lie algebraic properties of the orthonormal basis set and the fact that the set is closed under all possible commutations, to write the solution of this differential equation as product of the elements of the Lie set with some time-dependent coefficients.

Considering a basis set

$$\mathcal{L} = \{X_1, X_2, \dots, X_N\} \quad (46)$$

the elements of which satisfy the condition of Eq. (11), the assumed solution of the time-dependent propagator $\mathcal{U}(t)$ in Eq. (44) can be written as:

$$\mathcal{U}(t) = \prod_{i=1}^N \exp [g_i(t)X_i]; \quad g_i(0) = 0 \quad (47)$$

where $g_i(t)$ is a smooth function of time that gives the time variation of X_i element of the basis set \mathcal{L} .

By replacing Eqs. (12) and (47) in Eq. (44) and differentiation we obtain

$$\sum_{k=1}^N \dot{g}_k(t) \mathcal{E}_1^{k-1} X_k \mathcal{E}_k^N = -i \left(\sum_{j=1}^N \gamma_j X_j \right) \mathcal{E}_1^N \quad (48)$$

where

$$\mathcal{E}_p^q = \begin{cases} \prod_{i=p}^q \exp(g_i(t)X_i), & \text{if } q > p \\ \prod_{i=p}^q \exp(-g_i(t)X_i), & \text{if } q < p \end{cases} \quad (49)$$

Note that the products of exponentials in Eq. (49) are time-ordered, the order of which is dictated by the initial choice of the basis set \mathcal{L} .

By multiplying both sides of Eq. (48) by \mathcal{E}_{k-1}^1 we obtain

$$\sum_{k=1}^N \dot{g}_k(t) \mathcal{E}_1^{k-1} X_k \mathcal{E}_{k-1}^1 = -i \sum_{j=1}^N \gamma_j X_j \quad (50)$$

We can write this equation in vector and matrix form as

$$\mathcal{L}\Xi(\mathbf{g})\dot{\mathbf{g}}(t) = -i\mathcal{L}\boldsymbol{\gamma}^T \quad (51)$$

and therefore

$$\Xi(\mathbf{g})\dot{\mathbf{g}}(t) = -i\boldsymbol{\gamma}^T \quad (52)$$

Here the k^{th} column of the matrix $\Xi(\mathbf{g})$ will be ordered coefficients of \mathcal{L} in $\mathcal{E}_1^{k-1} X_k \mathcal{E}_{k-1}^1$. Construction of the matrix Ξ will be discussed in details in Section 2.3.1.

It is known from BCH (Baker-Campbell-Hausdorff) formula that the expression $\mathcal{E}_1^{k-1} X_k \mathcal{E}_{k-1}^1$ can be written using a series consisting of nested commutators:

$$e^X Y e^{-X} = Y + [X, Y] + \frac{[X, [X, Y]]}{2!} + \frac{[X, [X, [X, Y]]]}{3!} + \dots \quad (53)$$

A linear adjoint operator and its powers can be defined as:

$$\text{ad}_X^0(Y) = X, \quad \text{ad}_X(Y) = [X, Y], \quad \text{ad}_X^2(Y) = [X, [X, Y]], \dots \quad (54)$$

Therefore Eq. (53) can be written in terms of adjoint exponentials:

$$e^X Y e^{-X} = (e^{\text{ad}_X})Y \quad (55)$$

As it will be shown in Section 2.3.1, the series in Eq. (53) can be written as a closed-form generating function. For any two members, X_i and X_j of a basis set \mathcal{L} , that satisfy condition in Eq. (11) we have:

$$e^{g_i X_i} X_i e^{-g_j X_j} = \begin{cases} X_i, & \text{if } [X_i, X_j] = 0 \\ X_i \cosh(g) + [X_j, X_i] \sinh(g), & \text{if } [X_i, X_j] \neq 0 \end{cases} \quad (56)$$

It can be shown that the matrix Ξ which is an analytic function of time-dependent coefficients $g_i(t)$ is always invertible around time zero given the fact that at $t = 0$ Ξ is the Identity matrix and there is always a neighbourhood where it has non-zero determinant. Therefore, Eq. (52) can be re-arranged and be written as a system of differential equations as:

$$\dot{\mathbf{g}}(t) = -i \Xi^{-1}(\mathbf{g}) \boldsymbol{\gamma}^T \quad (57)$$

2.3.1. Example: single spin- $\frac{1}{2}$

In this section, a comprehensive example for the construction of Eq. (57) for a single spin- $\frac{1}{2}$ under a chirped pulse will be presented. Let us consider the Cartesian basis set as:

$$\mathcal{L} = \{\sigma_x, \sigma_y, \sigma_z\} \quad (58)$$

Although the order of the elements in the basis set can be arbitrarily chosen, we need to use the same order throughout our calculations.

We can write a set of cyclic commutations for a single spin- $\frac{1}{2}$ as follows:

$$[\sigma_x, \sigma_y] = i\sigma_z, \quad [\sigma_y, \sigma_z] = i\sigma_x, \quad [\sigma_z, \sigma_x] = i\sigma_y \quad (59)$$

the Hamiltonian of the system under a chirped pulse can be written as:

$$\mathcal{H}(t) = \Omega \sigma_z + C_x(t) \sigma_x + C_y(t) \sigma_y \quad (60)$$

and

$$\boldsymbol{\gamma} = [C_x(t), C_y(t), \Omega]. \quad (61)$$

where $C_x(t)$ and $C_y(t)$ are real and imaginary parts of the chirped pulse function in Eq. (4) respectively. This will be discussed in great details in Sections 2.3.2 and 3.2.

We consider the solution to Eq. (44) as follows:

$$\mathcal{U}(t) = e^{g_1(t)\sigma_x} e^{g_2(t)\sigma_y} e^{g_3(t)\sigma_z} \quad (62)$$

where $g_1(t)$, $g_2(t)$, and $g_3(t)$ are solutions of Eq. (57). This approach allows us to write the total propagator of the pulse sequence as an ordered product of time-dependent orthogonal rotation matrices, which is an attractive feature for the study and control of spin systems under field modulations [114] and is compatible with rotation-operator disentanglement approach [115].

The next step would be constructing the matrix $\Xi(g_1, g_2, \dots, g_N)$. According to Eq. (52) and the order of elements in the basis set \mathcal{L} , columns of $\Xi(g_1, g_2, \dots, g_N)$ can be obtained as functions of coefficients of corresponding elements of the basis.

Therefore three columns of $\Xi(g_1, g_2, \dots, g_N)$ will be obtained from:

$$\begin{cases} 1^{\text{st}} : & \sigma_x \\ 2^{\text{nd}} : & e^{g_1(t)\sigma_x} \sigma_y e^{-g_1(t)\sigma_x} \\ 3^{\text{rd}} : & e^{g_1(t)\sigma_x} e^{g_2(t)\sigma_y} \sigma_z e^{-g_1(t)\sigma_x} \end{cases} \quad (63)$$

It is clear that the 1st column is trivial. The 2nd column can be obtained via the application of Eq. (53) and the 3rd column is the nested version of Eq. (53). Note that this is a general approach and can be applied to any basis set that obeys the Lie algebra of SU(2^N) groups.

As an example, we derive the second column explicitly using Eq. (53) and show how the solution can be represented as a closed-form generating function presented in Eq. (56). The first four nested commutators used in Eq. (53) can be written as:

$$\begin{cases} [g_1(t)\sigma_x, \sigma_y] = i\sigma_z g_1(t) \\ [g_1(t)\sigma_x, [g_1(t)\sigma_x, \sigma_y]] = i\sigma_y g_1^2(t) \\ [g_1(t)\sigma_x, [g_1(t)\sigma_x, [g_1(t)\sigma_x, \sigma_y]]] = i\sigma_z g_1^3(t) \\ [g_1(t)\sigma_x, [g_1(t)\sigma_x, [g_1(t)\sigma_x, [g_1(t)\sigma_x, \sigma_y]]]] = i\sigma_y g_1^4(t) \end{cases} \quad (64)$$

therefore Eq. (53) can be written as a series and its closed-form generation function involving hyperbolic sines and cosines.

$$\Gamma = \begin{pmatrix} \cosh(g_2) \cosh(g_3) & & \\ -\sinh(g_1) \sinh(g_2) \cosh(g_3) + i \cosh(g_1) \sinh(g_3) & \cosh(g_1) \cosh(g_3) + i \sinh(g_1) \sinh(g_2) \sinh(g_3) & i \sinh(g_1) \cosh(g_2) \\ -i \cosh(g_1) \sinh(g_2) \cosh(g_3) - \sinh(g_1) \sinh(g_3) & i \sinh(g_1) \cosh(g_3) - \cosh(g_1) \sinh(g_2) \sinh(g_3) & \cosh(g_1) \cosh(g_2) \end{pmatrix} \quad (71)$$

$$\begin{aligned} (e^{ad_{g_1(t)\sigma_x}})\sigma_y &= \sigma_y + i\sigma_z g_1(t) + \frac{i\sigma_y g_1^2(t)}{2!} + \frac{i\sigma_z g_1^3(t)}{3!} + \dots \\ &= \sigma_y \cosh(g_1(t)) + i\sigma_z \sinh(g_1(t)) \end{aligned} \quad (65)$$

Eq. (65) can be written in a general form as Eq. (56).

Similarly, we can obtain elements of the last column of $\Xi(g_1, g_2, \dots, g_N)$:

$$\begin{aligned} (e^{ad_{g_1(t)\sigma_x}})(e^{ad_{g_2(t)\sigma_y}})\sigma_z &= i\sigma_x \sinh(g_2(t)) - i\sigma_y \sinh(g_1(t)) \\ &\quad \times \cosh(g_2(t)) + \sigma_z \cosh(g_1(t)) \\ &\quad \times \cosh(g_2(t)) \end{aligned} \quad (66)$$

Finally the matrix $\Xi(g)$ is obtained as:

$$\Xi = \begin{pmatrix} 1 & 0 & i \sinh(g_2(t)) \\ 0 & \cosh(g_1(t)) & -i \sinh(g_1(t)) \cosh(g_2(t)) \\ 0 & i \sinh(g_1(t)) & \cosh(g_1(t)) \cosh(g_2(t)) \end{pmatrix} \quad (67)$$

and the inverse of Ξ required for Eq. (57) is:

$$\begin{pmatrix} 1 & -\sinh(g_1(t)) \tanh(g_2(t)) & -i \cosh(g_1(t)) \tanh(g_2(t)) \\ 0 & \cosh(g_1(t)) & i \sinh(g_1(t)) \\ 0 & -i \sinh(g_1(t)) \operatorname{sech}(g_2(t)) & \cosh(g_1(t)) \operatorname{sech}(g_2(t)) \end{pmatrix}$$

Finally, using Eqs. (61) and (67) we can write Eq. (57) as:

$$\begin{pmatrix} \dot{g}_1 \\ \dot{g}_2 \\ \dot{g}_3 \end{pmatrix} = \begin{pmatrix} -iC_x + \tanh(g_2)(-\Omega \cosh(g_1) + iC_y \sinh(g_1)) \\ \Omega \sinh(g_1) - iC_y \cosh(g_1) \\ -\operatorname{sech}(g_2)(C_y \sinh(g_1) + i\Omega \cosh(g_1)) \end{pmatrix} \quad (68)$$

Which can be solved to obtain time-dependent coefficients, and hence the total time-dependent propagator $\mathcal{U}(t)$.

Of course it would be more desirable to have access to the structure of the density matrix as a result of such propagator. This can be achieved straightforwardly by the direct application of Eq. (62) in Eq. (43).

$$\rho(t) = e^{g_1(t)\sigma_x} e^{g_2(t)\sigma_y} e^{g_3(t)\sigma_z} \rho(0) e^{-g_3(t)\sigma_z} e^{-g_2(t)\sigma_y} e^{-g_1(t)\sigma_x} \quad (69)$$

where

$$\begin{aligned} \rho(t) &= c_1(t)\sigma_x + c_2(t)\sigma_y + c_3(t)\sigma_z, \\ \rho(0) &= c_1(0)\sigma_x + c_2(0)\sigma_y + c_3(0)\sigma_z \end{aligned} \quad (70)$$

Similar to previous sections, we can write Eq. (69) in vector and matrix form:

$$\begin{pmatrix} c_1(t) \\ c_2(t) \\ c_3(t) \end{pmatrix} = \Gamma(t) \begin{pmatrix} c_1(0) \\ c_2(0) \\ c_3(0) \end{pmatrix} \quad (71)$$

Here rows of the matrix Γ is obtained using the application of Eq. (56) in Eq. (69). The general form of Γ in Eq. (71) can be obtained explicitly as Eq. (72). Here the time-dependency of g_1, g_2 , and g_3 is dropped for simplicity. Using Eqs. (71) and (72) the state of the system at any time τ can be obtained by multiplying $\Gamma(\tau)$ by the initial state of the system.

2.3.2. Demo: Composite chirps for refocusing

In this section, the solution of spin dynamics for a sequence of chirped pulses will be presented. This sequence,

$$\begin{pmatrix} -i \cosh(g_2) \sinh(g_3) & i \sinh(g_2) \\ i \sinh(g_1) \cosh(g_3) + i \sinh(g_1) \sinh(g_2) \sinh(g_3) & -i \sinh(g_1) \cosh(g_2) \\ -i \cosh(g_1) \sinh(g_3) - \cosh(g_1) \sinh(g_2) \sinh(g_3) & \cosh(g_1) \cosh(g_2) \end{pmatrix} \quad (72)$$

introduced by Hwang et al. [17], offers an ideal refocusing of spins without any phase rolls across the spectral range of interest. It takes advantage of amplitude- and time-matching of three 180° chirped pulses in order to achieve zero net chemical shift evolution during the sequence and self-compensation with respect to variations of the B_1 field. Here the goal is to demonstrate how one can use the proposed approach in the previous section to compute and visualise the spin dynamics during such a pulse sequence.

For this example we consider a 1 ms - 2 ms - 1 ms sequence of chirped pulses with 200 kHz bandwidth. The whole sequence can be written as a sum of three chirped waveforms using Eqs. (8)–(10). Note that for this application all three pulses have the same bandwidth (ΔF) and RF amplitudes (ω_1), and for all of them $\phi_0 = 0$ and $\delta_f = 0$, but durations, τ_p and positions δ_t are different.

The total pulse sequence can therefore be written as:

$$S(t) = \omega_1 \sum_{i=1}^3 \exp \left[-2^{n+2} \left(\frac{t - \delta_t^{(i)}}{\tau_p^{(i)}} \right)^n + i \left(\frac{\pi \Delta F (t - \delta_t^{(i)})^2}{\tau_p^{(i)}} \right) \right] \quad (73)$$

The Hamiltonian of a single spin- $\frac{1}{2}$ under this sequence can be written as:

$$\mathcal{H}(t) = \Omega \sigma_z + C_x(t) \sigma_x + C_y(t) \sigma_y \quad (74)$$

where

$$C_x(t) = \omega_1 \sum_{i=1}^3 \exp \left[-2^{n+2} \left(\frac{t - \delta_t^{(i)}}{\tau_p^{(i)}} \right)^n \right] \cos \left[\left(\frac{\pi \Delta F (t - \delta_t^{(i)})^2}{\tau_p^{(i)}} \right) \right] \quad (75)$$

$$C_y(t) = \omega_1 \sum_{i=1}^3 \exp \left[-2^{n+2} \left(\frac{t - \delta_t^{(i)}}{\tau_p^{(i)}} \right)^n \right] \sin \left[\left(\frac{\pi \Delta F (t - \delta_t^{(i)})^2}{\tau_p^{(i)}} \right) \right]$$

Now we can write all 18 parameters of the sequence (3 pulses, 6 parameters each). $\omega_1 = 2\pi\mathcal{R}\mathcal{F}$ can be calculated using Eq. (35), where $\Delta F = 200000$ Hz and $\mathcal{Q} = 5$. δ_t is time offset of the centre-point of each pulse from the beginning of the sequence ($t = 0$). As none of the three pulses here have additional phase or frequency offset, these parameters will be set to zero. Therefore, a complete set of parameters for three chirped pulses in this sequence will be as follows:

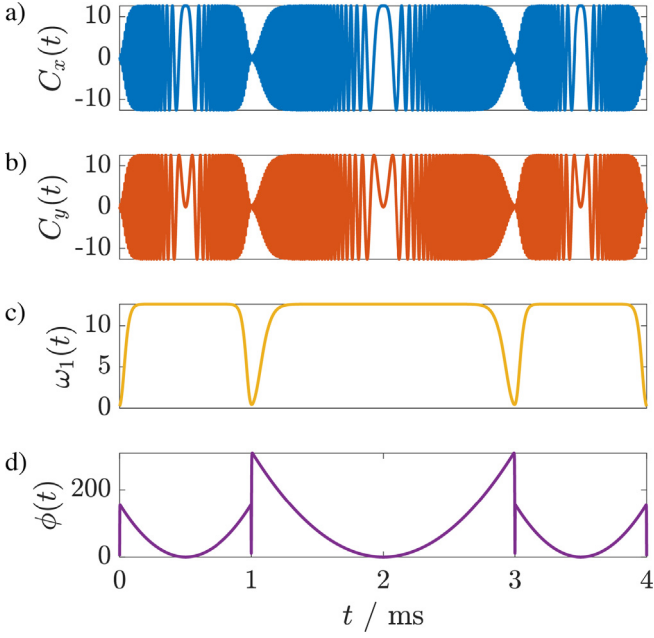


Fig. 4. Graphical representation of Cartesian ($C_x(t)$ and $C_y(t)$), and polar ($\omega_1(t)$ and $\phi(t)$) components of the composite refocusing chirped sequence, with parameters of Eq. (76). The unit for y-axis in (a), (b), and (c) is kHz and in (d) is radian.

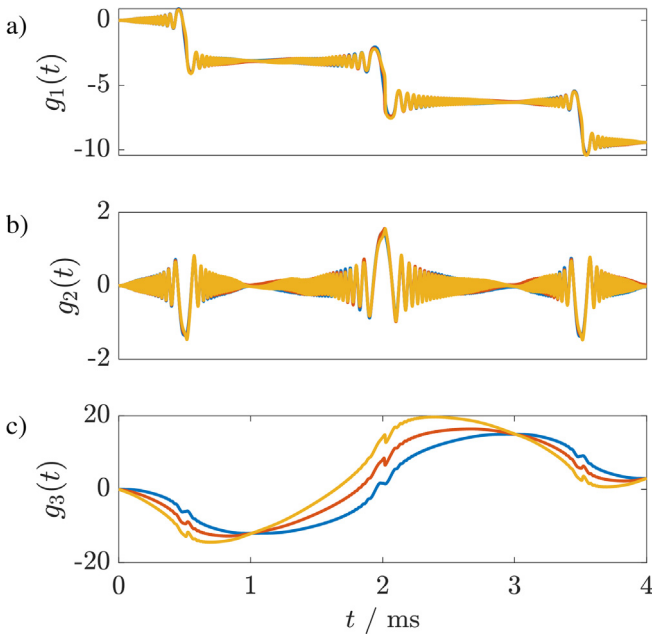


Fig. 5. Graphical representation of the time-variation of coefficients $g_1(t)$, $g_2(t)$, and $g_3(t)$ in Eq. (68) during the composite refocusing chirped sequence, with parameters of Eq. (76).

$$\left\{ \begin{array}{l} \omega_1 = [79267, 79267, 79267] \text{ (rad/s)} \\ \Delta F = [200000, 200000, 200000] \text{ (Hz)} \\ \tau_p = [0.001, 0.002, 0.001] \text{ (s)} \\ \phi_0 = [0, 0, 0] \text{ (rad)} \\ \delta_t = [0.0005, 0.0020, 0.0035] \text{ (s)} \\ \delta_f = [0, 0, 0] \text{ (Hz)} \end{array} \right. \quad (76)$$

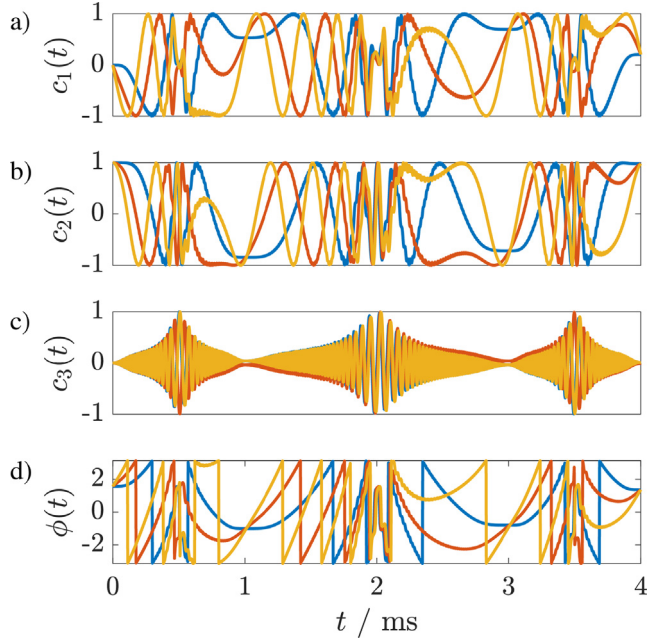


Fig. 6. Graphical representation of the time-variation of coefficients $c_1(t)$, $c_2(t)$, $c_3(t)$ in Eq. (71), and the phases $\phi(t) = \arctan(\frac{c_2(t)}{c_1(t)})$ during the composite refocusing chirped sequence, with parameters of Eq. (76).

Including these parameters in Eq. (75) results in the sequence shown in Fig. 4.

Now we can solve Eq. (68) for this system giving access to the solution of the unitary propagator for the whole sequence. This result can be incorporated in Eqs. (71) and (72) to have access to the time evolution of the density matrix for a single spin during this three-pulse sequence. For this example we consider the initial state of spins to be $|y\rangle$, i.e. in Eq. (71) $[c_1(0), c_2(0), c_3(0)]$ is $[0, 1, 0]$.

Fig. 5 shows the solutions for $g_1(t)$, $g_2(t)$, and $g_3(t)$ in Eq. (68) and therefore $U(t)$ in Eq. (62). Fig. 6 shows the time evolution of elements of the density matrix in Eq. (70) for three different offsets during the pulse sequence of Fig. 4. It is evident that the sequence gives perfect refocusing for signals although they undergo different trajectories during the sequence.

In Section 3.2 an application of this formalism will be presented for broadband excitation using the CHORUS sequence.

3. Some applications

3.1. Broadband homonuclear decoupling

In this section, we use the approach presented in Section 2.2.2 to describe and visualise the spin dynamics for a system of two coupled spin- $\frac{1}{2}$ s during the PSYCHE pulse element [116–120]. The best way to understand what makes a homonuclear decoupling element is to consider what we want to achieve using this pulse element and then relate those desired and undesired terms to specific members of the basis set. The main property of a J-refocusing pulse element, as in the PSYCHE experiment, as opposed to a conventional inversion/refocusing pulse, is that it acts on both types of interactions, chemical shift and J-coupling. Therefore in the context of a well-known spin-echo experiment, a homonuclear decoupling element is a refocusing (time-reversal) pulse for all interactions in the Hamiltonian. This is the key to distinguishing between the interactions of spins with the main magnetic field (chemical shifts) and interactions of spins with each other (scalar couplings). If we put this in the context of the basis set Eq. (31)

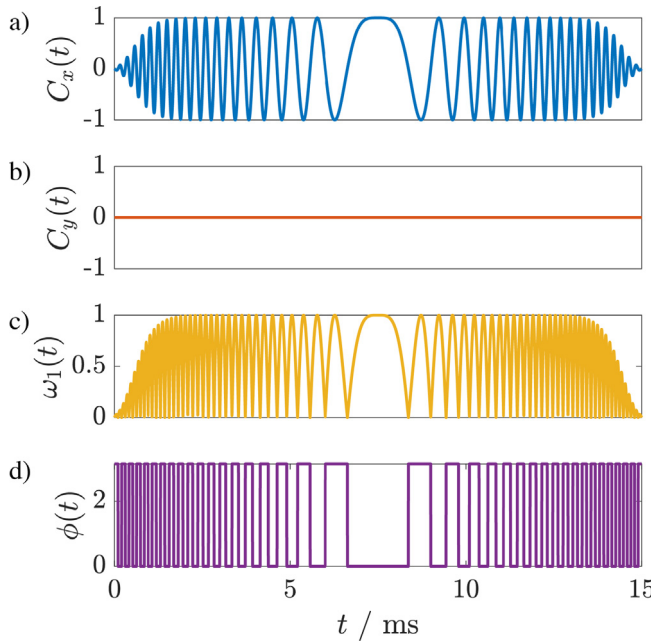


Fig. 7. Graphical representation of Cartesian ($C_x(t)$) and $C_y(t)$, and polar ($\omega_1(t)$ and $\phi(t)$) components of a saltire pulse with $\tau_p = 15$ ms, and $\Delta F = 10$ kHz.

and considering the relevant CTP selection is applied, all terms before and after the PSYCHE pulse element can be written as:

$$\begin{cases} P^+ \mapsto P^- \\ Q^+ \mapsto Q^- \\ P^+ Q_z \mapsto P^- Q_z \\ P_z Q^+ \mapsto P_z Q^- \end{cases} \quad (77)$$

Note that the effect of the PSYCHE pulse element can be seen as a collection of one-to-one maps between members of the basis set, in other words, Eq. (77) means that for each individual input (existing term before the pulse element) there is a unique output (emerging observable after the pulse element), and anything else generated during the pulse element should be suppressed. This assumption on the mechanism of the PSYCHE pulse element equips us with a useful approach to describe and visualise the spin dynamics during the PSYCHE pulse element. The PSYCHE method takes advantage of a combination of low flip angle double-sweep chirped (saltire) pulse and pulsed field gradient in order to achieve the objectives of Eq. (77). In this section, we consider the spin dynamics of a system of two spin-\$\frac{1}{2}\$s interacting via scalar \$J\$ coupling.

A saltire pulse is an average of two counter-sweeping unidirectional chirped pulses, that is, it is a pulse which simultaneously sweeps in frequency linearly in opposite directions over a frequency range ΔF in time τ_p . As shown in Fig. 7, this averaging changes the pulse from phase-modulated to amplitude modulated, modifying the appearance of the amplitude envelope. Note that for a saltire pulse:

$$\delta_t = \frac{\tau_p}{2}, \quad \phi_0 = 0, \quad \delta_f = 0, \quad t \in [0, \tau_p]$$

The general form of Eq. (4) for a saltire pulse can be written as:

$$S(t) = \frac{1}{2} \sum_{i=1}^2 \omega_i \exp \left[-2^{n+2} \left(\frac{t - \frac{\tau_p}{2}}{\tau_p} \right)^n + i \left(\frac{(-1)^i \pi \Delta F (t - \frac{\tau_p}{2})^2}{\tau_p} \right) \right]$$

which turns the pulse into an amplitude-modulated pulse:

$$S(t) = \omega_1 \exp \left[-2^{n+2} \left(\frac{t - \frac{\tau_p}{2}}{\tau_p} \right)^n \right] \cos \left[\frac{\pi \Delta F (t - \frac{\tau_p}{2})^2}{\tau_p} \right] \quad (78)$$

The Hamiltonian for two coupled spin-\$\frac{1}{2}\$s in the presence of a saltire chirp pulse and a simultaneous pulsed field gradient can be written as:

$$\mathcal{H}(t) = \Omega_P P_z + \Omega_Q Q_z + \pi J (P^- Q^+ + P^+ Q^- + 2P_z Q_z) + \beta (P^+ + Q^+ + P^- + Q^-) + \Omega_g(z) (P_z + Q_z) \quad (79)$$

where

$$\beta = \frac{1}{2} \omega_1 \exp \left[-2^{n+2} \left(\frac{t - \delta_t}{\tau_p} \right)^n \right] \cos \left[\frac{\pi \Delta F (t - \frac{\tau_p}{2})^2}{\tau_p} \right] \quad (80)$$

and $\Omega_g(z)$ is a frequency offset induced by the pulsed field gradient as in Eq. (40).

Again, similar to the zero quantum suppression, in order to avoid unnecessary signal loss due to diffusion or excessive spatial encoding we adjust the strength of gradient $G(z)$ so that $\Omega_g(z)$ varies in the range $-\pi \Delta F$ to $+\pi \Delta F$.

Finally, the array of the Hamiltonian coefficients for the PSYCHE pulse element can be written as:

$$\gamma = [\Omega_P + \Omega_g(z), \Omega_Q + \Omega_g(z), \pi J, \pi J, \sqrt{2}\beta, \sqrt{2}\beta, \sqrt{2}\beta, \sqrt{2}\beta, 0, 0, 0, 0, 0, 0, 0] \quad (81)$$

Now including these in Eq. (34) we can set a system of ODEs for this system. We need to replace Ω_P and Ω_Q with $\Omega_P + \Omega_g(z)$ and $\Omega_Q + \Omega_g(z)$ respectively. Additionally we have:

$$\mathcal{J} = \pi J, \quad \mathcal{B} = \sqrt{2}\beta, \quad \Sigma = \Omega_P + \Omega_Q + 2\Omega_g(z), \quad \Delta = \Omega_P - \Omega_Q$$

Moreover as the saltire pulse is an amplitude modulated pulse (has only the real part), $\mathcal{B} = \mathcal{B}^*$ and matrix Γ in Eq. (21) is not hermitian, but symmetric. Additionally, as a result of the pulse being amplitude-modulated the \mathcal{RF} dependence of the flip-angle (α) is not asymptotic and can be obtained by the integration of the time-envelope of the saltire pulse:

$$\mathcal{RF}_{max} = \left(\frac{\alpha}{360} \right) \sqrt{\frac{2\Delta F}{\tau_p}} \quad (82)$$

In order to see the mechanism of PSYCHE experiment it is crucial to see trajectories of different elements of the basis set and observe how desired terms are prepared for detection and undesired paths are suppressed. For this we need to know the status of the system before the saltire pulse. Since there is only one 90° pulse before the saltire pulse, some 180° pulses, and some arbitrary delay we can consider that before the PSYCHE pulse element we have only single quantum terms which can be in the form of a mixture of in-phase (e.g. P^+) and anti-phase (e.g. $P^+ Q_z$) terms. Of course, during the low-amplitude saltire pulse all other coherence orders will be generated. The idea here is to see how the combination of a low-flip angle saltire pulse and a pulsed field gradient results in an efficient filtration and attenuation of unwanted terms and achieving objectives in Eq. (77).

Without loss of generality, let us consider a case when we feed the PSYCHE pulse element, consisting of a saltire pulse and a simultaneous pulsed field gradient, with P^+ only, i.e. at the beginning of the event $g_7(0) = 1$ and all other coefficients are 0. By looking at Eq. (77) it is clear that the desired output after pulse element should be P^- , i.e. we want to maximise $g_6(\tau_p)$ while suppressing all other terms as much as possible. This case study is carried out by considering two independent characteristics of the pulse element: spatiotemporal averaging and low-flip angle excitation. Note that due to the CTP selection and detection of observable terms with negative coherence order we are not interested in single quantum

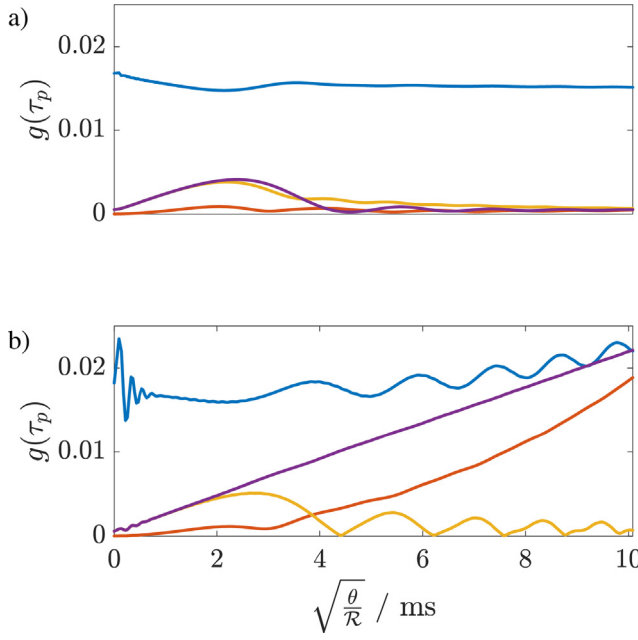


Fig. 8. Graphical representation of 4 terms $g_6(\tau_p)$ (blue), $g_8(\tau_p)$ (red), $g_{10}(\tau_p)$ (orange), and $g_{12}(\tau_p)$ (purple), corresponding to terms on the right side of Eq. (77), P^-, Q^-, P^-Q_z , and P_zQ^- respectively as in the basis set of Eq. (31) as a function of ξ (Eq. (42)); a) in the presence, and b) in the absence of the pulsed field gradient. In both cases $\alpha = 15^\circ$. (For interpretation of the references to colour in this figure legend, the reader is referred to the web version of this article.)

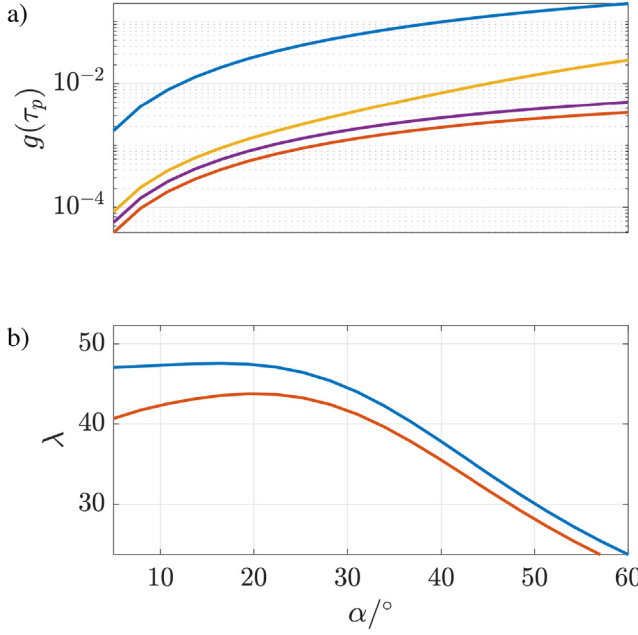


Fig. 9. a) Graphical representation of the intensities of 4 terms $g_6(t)$ (blue), $g_8(t)$ (red), $g_{10}(t)$ (orange), and $g_{12}(t)$ (purple), corresponds to terms on the right side of Eq. (77), P^-, Q^-, P^-Q_z , and P_zQ^- respectively as in the basis set of Eq. (31) versus flip angle (α), b) λ (Eq. (83)) with (red) and without (blue) the penalty term; $\tau_p = 30$ ms, $\Delta F = 10$ kHz, $\Delta = 200$ Hz, and $J = 10$ Hz. (For interpretation of the references to colour in this figure legend, the reader is referred to the web version of this article.)

terms with positive coherences at the end of the pulse, P^+, Q^+, P^+Q_z , and P_zQ^+ , corresponding to $g_7(\tau_p), g_9(\tau_p), g_{11}(\tau_p)$, and $g_{13}(\tau_p)$ coefficients respectively. The total objectives of the experiment therefore are: i) maximising P^- corresponding to $g_6(\tau_p)$ as the desired output; ii) minimising other observable

(single quantum) terms (Q^-, P^-Q_z , and P_zQ^-) corresponding to $g_8(\tau_p), g_{10}(\tau_p), g_{12}(\tau_p)$, and iii) suppression of terms with zero quantum coherences (P_z, Q_z, P^-Q^+, P^+Q^- , and P_zQ_z) corresponding to $g_1(\tau_p)$ to $g_5(\tau_p)$ respectively and double quantum coherences (P^-Q^- and P^+Q^+) corresponding to $g_{14}(\tau_p)$ and $g_{15}(\tau_p)$. Fig. 8 shows the variation of these 4 terms at the end of a saltire pulse in the presence and absence of a pulsed field gradient as a function of ξ (Eq. (42)).

Fig. 9(a) shows the flip angle dependence of these 4 terms. It is evident that although the ratio of wanted term P^- to unwanted terms (Q^-, P^-Q_z , and P_zQ^-) is much higher for smaller flip angles, but on the downside, the magnitude of the wanted signal will be significantly smaller. Therefore, it is sensible to seek a compromise for the best suppression of unwanted signals and the best possible sensitivity of the desired signal. For this purpose let us define a parameter λ as:

$$\lambda = 3 \frac{g_6(\tau_p)}{\|a\|}, \quad a = [g_8(\tau_p), g_{10}(\tau_p), g_{12}(\tau_p)] \quad (83)$$

The blue graph in Fig. 9(b) shows the value of parameter λ as a function of flip angle. Of course we are interested in a flip angle that maximises both λ and $g_6(\tau_p)$, therefore we can rewrite the λ as:

$$\lambda = 3 \frac{g_6(\tau_p)}{\|a\|} + \ln(g_6(\tau_p)) \quad (84)$$

Here the term $\ln(g_6(\tau_p))$ acts as a penalty term to avoid unnecessary signal loss. The red graph in Fig. 9(b) represents the variation of the modified λ as a function of flip angle α , which shows an optimal flip angle of $\sim 20^\circ$. Of course, in Eq. (84) data was considered noiseless and only signal-to-artefact ratio was taken into account. In reality with noisy data one can use larger flip angle, as long as the magnitude of unwanted signals remains within the noise variance.

Fig. 10 shows time-variation of all 15 coefficients of the members of the basis set in Eq. (31) at different parts of the active volume of the sample during a PSYCHE pulse element. The idea of phase variation leading to efficient spatiotemporal averaging is obvious from insets $g_1(t)$ to $g_5(t)$ in Fig. 10. On the other hand, it leads to non-zero averaging for $g_6(\tau_p), g_8(\tau_p), g_{10}(\tau_p), g_{12}(\tau_p)$.

3.2. Broadband excitation

In this section, we use the approach presented in Section 2.3.1 to describe and visualise the spin dynamics of a group of non-interacting spin- $\frac{1}{2}$ s during the CHORUS [29,28,31] pulse sequence. The whole sequence can be written as a sum of three chirped waveforms as in Eqs. (8)–(10). Note that all three pulses have the same bandwidth ΔF , and for all of them $\phi_0 = 0$ and $\delta_f = 0$, but duration, τ_p , position, δ_t , and \mathcal{RF} amplitude, ω_1 , are different.

The total pulse sequence can therefore be written as:

$$C(t) = \sum_{i=1}^3 \omega_1^{(i)} \exp \left[-2^{n+2} \left(\frac{t - \delta_t^{(i)}}{\tau_p^{(i)}} \right)^n + i \left(\frac{\pi \Delta F (t - \delta_t^{(i)})^2}{\tau_p^{(i)}} \right) \right] \quad (85)$$

The Hamiltonian of a single spin- $\frac{1}{2}$ under CHORUS sequence is:

$$\mathcal{H}(t) = \Omega \sigma_z + C_x(t) \sigma_x + C_y(t) \sigma_y \quad (86)$$

where

$$C_x(t) = \sum_{i=1}^3 \omega_1^{(i)} \exp \left[-2^{n+2} \left(\frac{t - \delta_t^{(i)}}{\tau_p^{(i)}} \right)^n \right] \cos \left[\left(\frac{\pi \Delta F (t - \delta_t^{(i)})^2}{\tau_p^{(i)}} \right) \right]$$

$$C_y(t) = \sum_{i=1}^3 \omega_1^{(i)} \exp \left[-2^{n+2} \left(\frac{t - \delta_t^{(i)}}{\tau_p^{(i)}} \right)^n \right] \sin \left[\left(\frac{\pi \Delta F (t - \delta_t^{(i)})^2}{\tau_p^{(i)}} \right) \right]$$

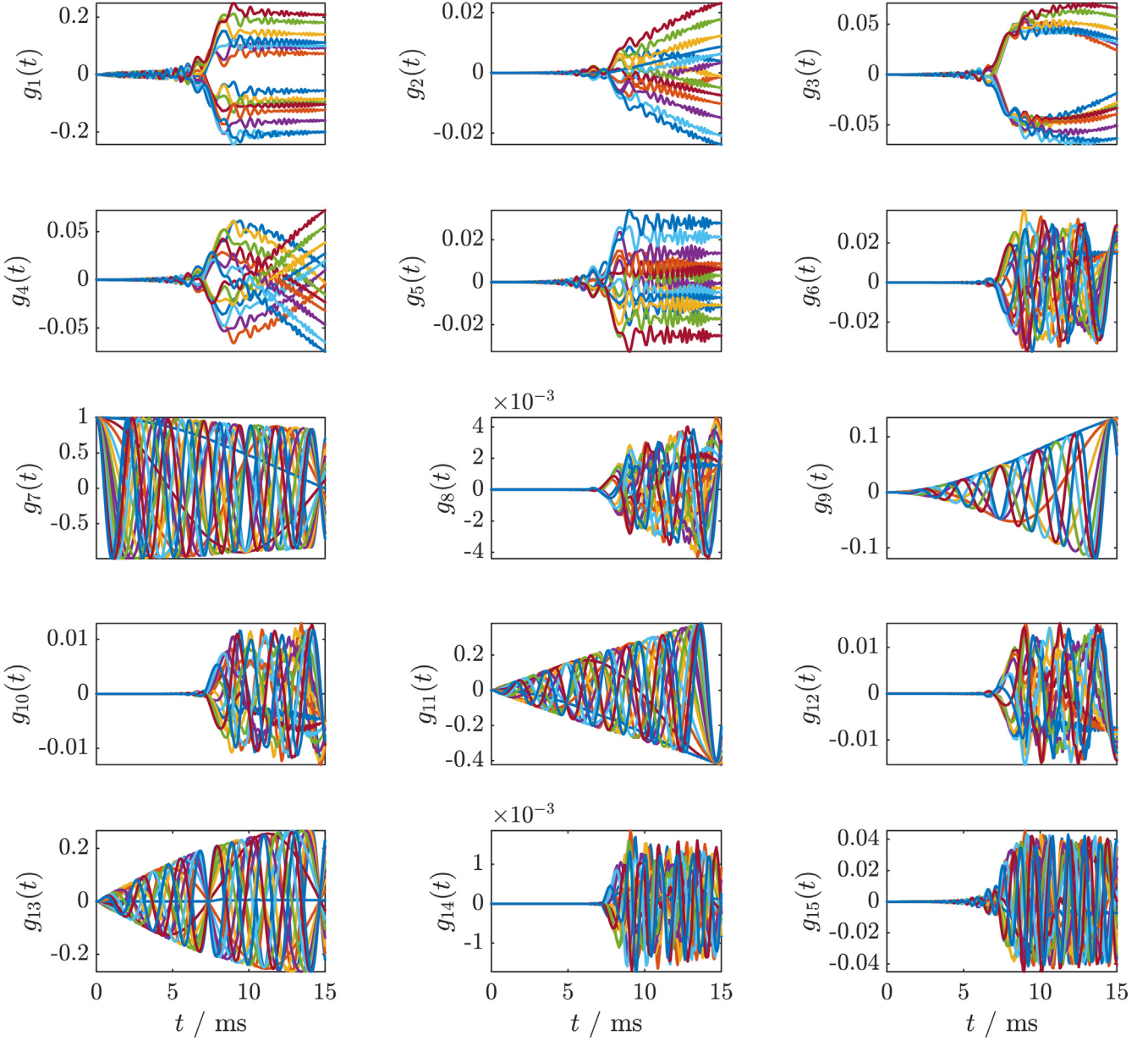


Fig. 10. Graphical representation of time-dependent coefficients $g_1(t)$ to $g_{15}(t)$ during a PSYCHE pulse element; different colours represent time-evolution of terms at different parts of the active volume of the sample.

The relative timings for the CHORUS sequence are unique: $\tau_p^{(2)} = \frac{\tau_p^{(1)}}{2} + \tau_p^{(3)}$ with a delay between two 180° pulses equal to $\frac{\tau_p^{(1)}}{2}$. Therefore for the full CHORUS sequence $t \in [0, 2(\tau_p^{(1)} + \tau_p^{(3)})]$. For example, if the durations of the first (90°) and the last (180°) chirped pulses are $500 \mu\text{s}$ and 1 ms respectively, the total sequence will be 3 ms long.

Here we use Wei-Norman Lie algebra as presented in Section 2.3. We know the general form of matrix Ξ (Eq. (67)) and its inverse, which is independent of the coefficients of the basis set in the Hamiltonian. Now we can solve Eq. (68) for this system giving access to the solution of the unitary propagator for the whole sequence. This result can be incorporated in Eqs. (71) and (72) to have access to the time evolution of the density matrix for single spin during CHORUS sequence.

An example set of parameters for the CHORUS sequence shown in Fig. 11 is written as:

$$\begin{cases} \boldsymbol{\omega}_1 = [40787, 86832, 97081] \text{ (rad/s)} \\ \Delta F = [300000, 300000, 300000] \text{ (Hz)} \\ \boldsymbol{\tau}_p = [0.0005, 0.00125, 0.001] \text{ (s)} \\ \boldsymbol{\phi}_0 = [0, 0, 0] \text{ (rad)} \\ \delta_t = [0.00025, 0.001125, 0.0025] \text{ (s)} \\ \delta_f = [0, 0, 0] \text{ (Hz)} \end{cases} \quad (87)$$

Fig. 12 shows the solution of Eq. (68) for $g_1(t)$, $g_2(t)$, and $g_3(t)$, and Fig. 13 shows the time-variation of coefficients $c_1(t)$, $c_2(t)$, $c_3(t)$ in Eq. 71, and the phases $\phi(t) = \arctan\left(\frac{c_2(t)}{c_1(t)}\right)$ during the CHORUS sequence.

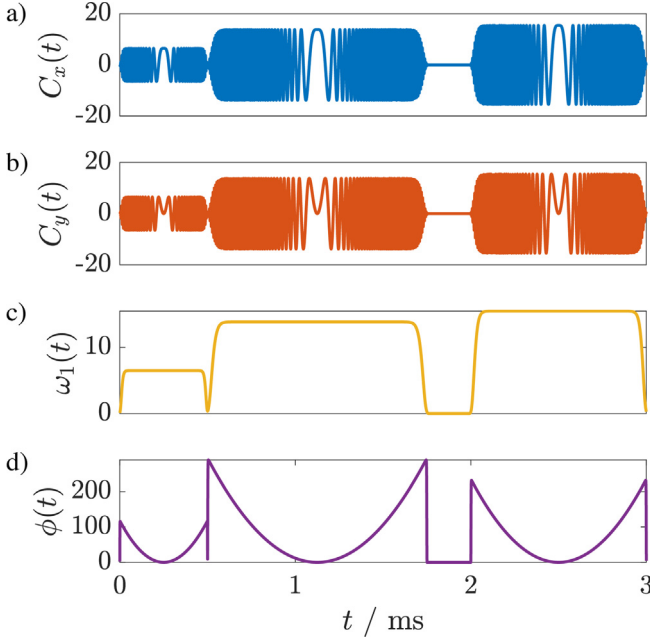


Fig. 11. Graphical representation of Cartesian ($C_x(t)$ and $C_y(t)$), and polar ($\omega_1(t)$ and $\phi(t)$) components of the composite refocusing chirped sequence, with parameters of Eq. (87).

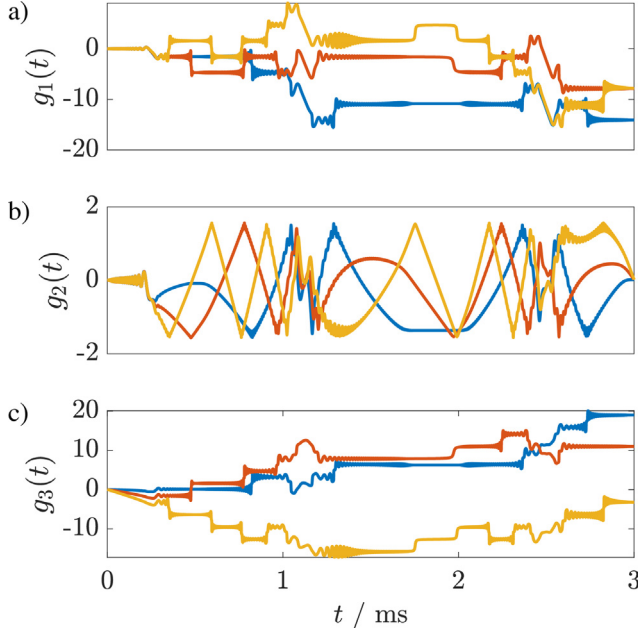


Fig. 12. Graphical representation of the time-variation of coefficients $g_1(t)$, $g_2(t)$, and $g_3(t)$ in Eq. (68) during the CHORUS sequence, with parameters of Eq. (76).

One remaining issue here is the presence of some residual phase roll across the spectrum. In previous works [29,31] it has been proposed that this problem can be fixed by fitting a polynomial function to the phase response of the sequence and add that function directly to the phase of the first pulse (90°). Here, due to the additional degree of freedom of the generalised chirped pulse, one can approach and solve this problem more efficiently by tweaking the pulse parameters. First, let us write $C_x(t)$ and $C_y(t)$ for the CHORUS sequence in their most general forms.

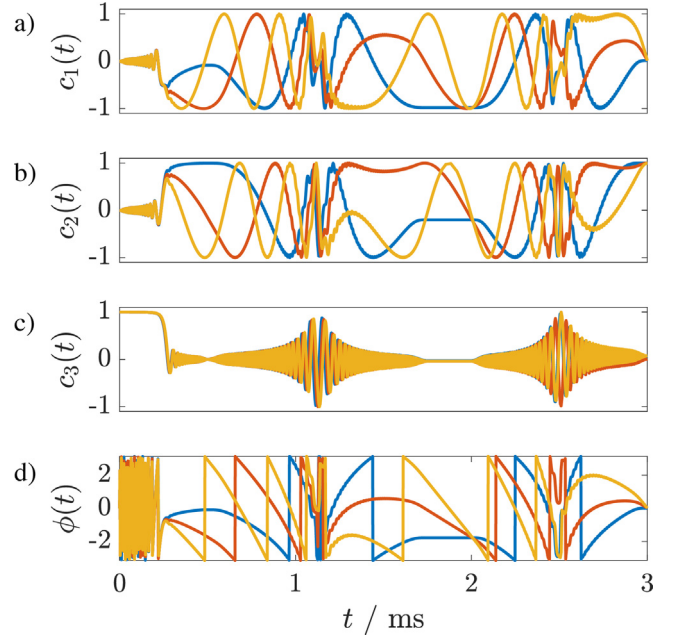


Fig. 13. Graphical representation of the time-variation of coefficients $c_1(t)$, $c_2(t)$, $c_3(t)$ in Eq. (71), and the phases $\phi(t) = \arctan\left(\frac{c_2(t)}{c_1(t)}\right)$ during the CHORUS sequence, with parameters of Eq. (76).

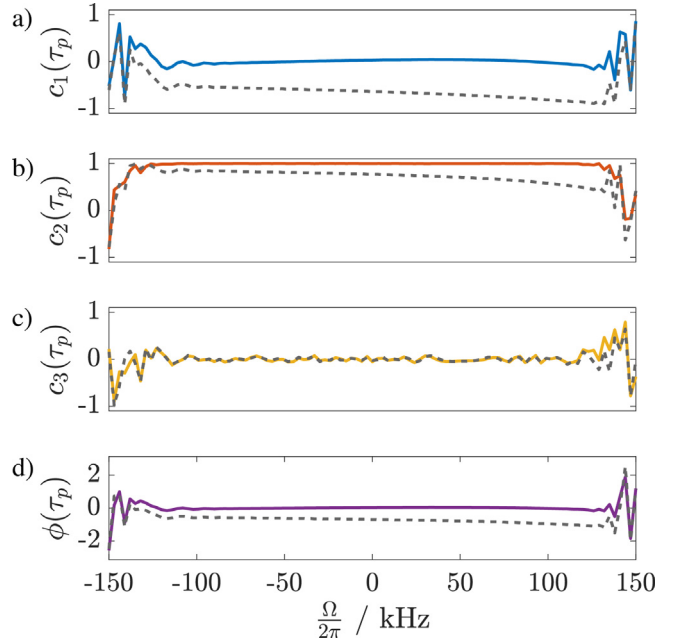


Fig. 14. Graphical representation of the excitation profile the CHORUS pulse sequence; $c_1(\tau_p)$, $c_2(\tau_p)$, $c_3(\tau_p)$ in Eq. (71), and the phases $\phi(\tau_p) = \arctan\left(\frac{c_2(\tau_p)}{c_1(\tau_p)}\right)$ before and after the correction with pulse sequence parameters of Eqs. (87) and (91) respectively.

$$C_x(t) = \sum_{i=1}^3 \omega_1^{(i)} \exp \left[-2^{n+2} \left(\frac{t - \delta_t^{(i)}}{\tau_p^{(i)}} \right)^n \right] \cos \left[\phi_0^{(i)} + \frac{\pi \Delta F (t - \delta_t^{(i)})^2}{\tau_p^{(i)}} - 2\pi \delta_f^{(i)} (t - \delta_t^{(i)}) \right] \quad (88)$$

and

$$\begin{aligned} C_y(t) &= \sum_{i=1}^3 \omega_i^{(i)} \exp \left[-2^{n+2} \left(\frac{t - \delta_t^{(i)}}{\tau_p^{(i)}} \right)^n \right] \\ &\sin \left[\phi_0^{(i)} + \frac{\pi \Delta F (t - \delta_t^{(i)})^2}{\tau_p^{(i)}} - 2\pi \delta_f^{(i)} (t - \delta_t^{(i)}) \right] \end{aligned} \quad (89)$$

It can be seen that the variation of overall phase ϕ_0 and frequency offset δ_f of the 90° pulse in this 3-pulse sequence can lead to a controllable variation of signal phase across the spectrum. This additional degree of freedom can be harnessed to apply non-linear phase correction instead of the method described in [29,31] relying on polynomial fitting.

The whole approach can be written as a simple optimisation as:

$$\underset{\phi_0, \delta_f}{\operatorname{argmin}} \operatorname{Var}[\phi(\Omega)] \quad (90)$$

where Var represents the variance and $\phi(\Omega)$ is the phase of signals at the end of the sequence as a function of the resonance offset Ω .

Fig. 14 shows excitation profiles of CHORUS pulse sequence by plotting coefficients of the density matrix at the end of the sequence i.e. $c_1(\tau_p), c_2(\tau_p), c_3(\tau_p)$, $\tau_p = 2(\tau_p^{(1)} + \tau_p^{(3)})$, as a function of the resonance offset Ω .

The set of sequence parameters of Eq. (87) after tweaking ϕ_0 and δ_f is:

$$\left\{ \begin{array}{l} \omega_1 = [40787, 86832, 97081] \text{ (rad/s)} \\ \Delta F = [300000, 300000, 300000] \text{ (Hz)} \\ \tau_p = [0.0005, 0.00125, 0.001] \text{ (s)} \\ \phi_0 = [-0.0668, 0.1878, -0.1404] \text{ (rad)} \\ \delta_t = [0.00025, 0.001125, 0.0025] \text{ (s)} \\ \delta_f = [-200, 0, 0] \text{ (Hz)} \end{array} \right. \quad (91)$$

Finally, Eq. (68) can be solved for a range of RF amplitudes in order to assess the insensitivity of the CHORUS pulse sequence to variations of the B_1 field. **Fig. 15** shows the magnitude of excited signal as functions of resonance offset and variation of nominal RF amplitude, using a set of parameters as in Eq. 91.

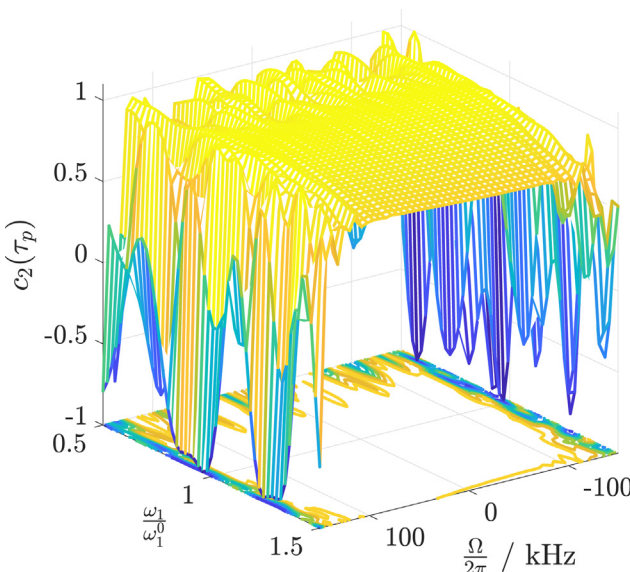


Fig. 15. 3D plots showing the y-magnetization at the end of the CHORUS sequence ($c_2(\tau_p)$) as a function of resonance offset (Ω) and relative RF amplitude ($\frac{\omega_1}{\omega_0}$).

4. Conclusion

In the present work, a generalised expression for chirped pulses was introduced that allows pulse sequences consisting of multiple chirped pulses to be written as a single time-continuous waveform. Two mathematical approaches based on Liouville-von Neumann equation and Wei-Norman Lie algebra were presented to calculate and visualise spin dynamics during chirped pulses. Full mathematical treatments were presented on comprehensive examples, and numerical calculations via solutions of ordinary differential equations were presented for broadband homonuclear decoupling using the PSYCHE method and broadband excitation using the CHORUS sequence. Methods proposed in this Perspective have the potential to find applications in NMR, ESR, MRI, and *in vivo* MRS, where design, simulation, and optimisation of experiments and optimal control of spin systems via parametrised waveforms like swept-frequency pulses are desired.

Declaration of Competing Interest

The authors declare that they have no known competing financial interests or personal relationships that could have appeared to influence the work reported in this paper.

Acknowledgements

I am grateful to the Royal Society for a University Research Fellowship and a University Research Fellow Enhancement Award (Grant Nos. URF|R1|180233 and RGF|EA|181018). I wish to thank Dr. Jean-Nicolas Dumez, Jean-Baptiste Verstraete, and Jonathan Yong for useful comments on the manuscript. I especially thank anonymous reviewers for their comprehensive comments and constructive criticisms.

References

- [1] T. Kato, On the adiabatic theorem of quantum mechanics, *J. Phys. Soc. Jpn* 5 (6) (1950) 435–439.
- [2] A. Tannus, M. Garwood, Adiabatic pulses, *NMR Biomed.* 10 (8) (1997) 423–434.
- [3] M. Garwood, L. DelaBarre, The return of the frequency sweep: designing adiabatic pulses for contemporary nmr, *J. Magn. Reson.* 153 (2) (2001) 155–177.
- [4] Y.A. Tesiram, M.R. Bendall, Universal equations for linear adiabatic pulses and characterization of partial adiabaticity, *J. Magn. Reson.* 156 (1) (2002) 26–40.
- [5] C.A. Meriles, D. Sakellariou, A. Pines, Broadband phase modulation by adiabatic pulses, *J. Magn. Reson.* 164 (1) (2003) 177–181.
- [6] R. Tycko, Broadband population inversion, *Phys. Rev. Lett.* 51 (9) (1983) 775–777.
- [7] J. Baum, R. Tycko, A. Pines, Broadband population inversion by phase modulated pulses, *J. Chem. Phys.* 79 (9) (1983) 4643–4644.
- [8] R. Tycko, E. Schneider, A. Pines, Broadband population inversion in solid state nmr, *J. Chem. Phys.* 81 (2) (1984) 680–688.
- [9] J. Baum, R. Tycko, A. Pines, Broadband and adiabatic inversion of a two-level system by phase-modulated pulses, *Phys. Rev. A* 32 (6) (1985) 3435–3447.
- [10] C.J. Hardy, W.A. Edelstein, D. Vatis, Efficient adiabatic fast passage for nmr population-inversion in the presence of radiofrequency field inhomogeneity and frequency offsets, *J. Magn. Reson.* 66 (3) (1986) 470–482.
- [11] M.R. Bendall, M. Garwood, K. Ugurbil, D.T. Pegg, Adiabatic refocusing pulse which compensates for variable rf power and off-resonance effects, *Magn. Reson. Med.* 4 (5) (1987) 493–499.
- [12] J.-M. Böhnen, I. Burghardt, M. Rey, G. Bodenhausen, Frequency-modulated "chirp" pulses for broadband inversion recovery in magnetic resonance, *J. Magn. Reson.* 90 (1) (1990) 183–191.
- [13] T. Fujiwara, K. Nagayama, Optimized frequency/phase-modulated broadband inversion pulses, *J. Magn. Reson.* 86 (3) (1990) 584–592.
- [14] Y. Ke, D.G. Schupp, M. Garwood, Adiabatic dante sequences for b1-insensitive narrowband inversion, *J. Magn. Reson.* 96 (3) (1992) 663–669.
- [15] Ě. Kupčík, R. Freeman, Stretched adiabatic pulses for broadband spin inversion, *J. Magn. Reson. A* 117 (2) (1995) 246–256.
- [16] Ě. Kupčík, R. Freeman, Optimized adiabatic pulses for wideband spin inversion, *J. Magn. Reson. A* 118 (2) (1996) 299–303.
- [17] T.L. Hwang, P.C. van Zijl, M. Garwood, Broadband adiabatic refocusing without phase distortion, *J. Magn. Reson.* 124 (1) (1997) 250–254.

- [18] T.L. Hwang, P.C. van Zijl, M. Garwood, Fast broadband inversion by adiabatic pulses, *J. Magn. Reson.* 133 (1) (1998) 200–203.
- [19] Ē. Kupčē, R. Freeman, Compensated adiabatic inversion pulses: broadband inept and hsqc, *J. Magn. Reson.* 187 (2) (2007) 258–265.
- [20] K.J. Harris, A. Lupulescu, B.E. Lucier, L. Frydman, R.W. Schurko, Broadband adiabatic inversion pulses for cross polarization in wideline solid-state nmr spectroscopy, *J. Magn. Reson.* 224 (2012) 38–47.
- [21] P.E. Spindler, S.J. Glaser, T.E. Skinner, T.F. Prisner, Broadband inversion peldor spectroscopy with partially adiabatic shaped pulses, *Angew. Chem. Int. Ed. Engl.* 52 (12) (2013) 3425–3429.
- [22] D. Kunz, Use of frequency-modulated radiofrequency pulses in mr imaging experiments, *Magn. Reson. Med.* 3 (3) (1986) 377–384.
- [23] J.-M. Böhlen, M. Rey, G. Bodenhausen, Refocusing with chirped pulses for broadband excitation without phase dispersion, *J. Magn. Reson.* 84 (1) (1989) 191–197.
- [24] V.L. Ermakov, G. Bodenhausen, Broadband excitation in magnetic resonance by self-refocusing doubly frequency-modulated pulses, *Chem. Phys. Lett.* 204 (3–4) (1993) 375–380.
- [25] V.L. Ermakov, J.M. Böhlen, G. Bodenhausen, Improved schemes for refocusing with frequency-modulated chirp pulses, *J. Magn. Reson. A* 103 (2) (1993) 226–229.
- [26] T.E. Skinner, P.M.L. Robitaille, Adiabatic excitation using sin² amplitude and cos² frequency modulation functions, *J. Magn. Reson. A* 103 (1) (1993) 34–39.
- [27] K.E. Cano, M.A. Smith, A.J. Shaka, Adjustable, broadband, selective excitation with uniform phase, *J. Magn. Reson.* 155 (1) (2002) 131–139.
- [28] J.E. Power, M. Foroozandeh, R.W. Adams, M. Nilsson, S.R. Coombes, A.R. Phillips, G.A. Morris, Increasing the quantitative bandwidth of nmr measurements, *Chem. Commun.* 52 (2016) 2916–2919.
- [29] J.E. Power, M. Foroozandeh, P. Moutzouri, R.W. Adams, M. Nilsson, S.R. Coombes, A.R. Phillips, G.A. Morris, Very broadband diffusion-ordered nmr spectroscopy: (19)f dosy, *Chem. Commun.* 52 (2016) 6892–6894.
- [30] N. Khaneja, Chirp excitation, *J. Magn. Reson.* 282 (2017) 32–36.
- [31] M. Foroozandeh, M. Nilsson, G.A. Morris, Improved ultra-broadband chirp excitation, *J. Magn. Reson.* 302 (2019) 28–33.
- [32] K. Ugurbil, M. Garwood, M. Robin Bendall, Amplitude- and frequency-modulated pulses to achieve 90° plane rotations with inhomogeneous b1 fields, *J. Magn. Reson.* 72 (1) (1987) 177–185.
- [33] K. Ugurbil, M. Garwood, A.R. Rath, Optimization of modulation functions to improve insensitivity of adiabatic pulses to variations in b1 magnitude, *J. Magn. Reson.* 80 (3) (1988) 448–469.
- [34] H. Merkle, H. Wei, M. Garwood, K. Ugurbil, B1-insensitive heteronuclear adiabatic polarization transfer for signal enhancement, *J. Magn. Reson.* 99 (3) (1992) 480–494.
- [35] M. Garwood, B. Nease, Y. Ke, R.A. De Graaf, H. Merkle, Simultaneous compensation for b1 inhomogeneity and resonance offsets by a multiple-quantum nmr sequence using adiabatic pulses, *J. Magn. Reson. A* 112 (1995) 272–274.
- [36] R.A. de Graaf, Y. Luo, M. Garwood, K. Nicolay, B1-insensitive, single-shot localization and water suppression, *J. Magn. Reson. B* 113 (1) (1996) 35–45.
- [37] R.A. de Graaf, K. Nicolay, M. Garwood, Single-shot, b1-insensitive slice selection with a gradient-modulated adiabatic pulse, biss-8, *Magn. Reson. Med.* 35 (5) (1996) 652–657.
- [38] P.C.M. van Zijl, T.-L. Hwang, M. O’Neil Johnson, M. Garwood, Optimized excitation and automation for high-resolution nmr using b1-insensitive rotation pulses, *J. Am. Chem. Soc.* 118 (23) (1996) 5510–5511.
- [39] T.B. Smith, K.S. Nayak, Reduced field of view mri with rapid, b1-robust outer volume suppression, *Magn. Reson. Med.* 67 (5) (2012) 1316–1323.
- [40] T. Fujiwara, T. Anai, N. Kurihara, K. Nagayama, Frequency-switched composite pulses for decoupling carbon-13 spins over ultrabroad bandwidths, *J. Magn. Reson. A* 104 (1) (1993) 103–105.
- [41] R. Fu, G. Bodenhausen, Broadband decoupling in nmr with frequency-modulated ‘chirp’ pulses, *Chem. Phys. Lett.* 245 (4–5) (1995) 415–420.
- [42] R.Q. Fu, G. Bodenhausen, Ultra-broadband decoupling, *J. Magn. Reson. A* 117 (2) (1995) 324–325.
- [43] Ē. Kupčē, R. Freeman, Adiabatic pulses for wideband inversion and broadband decoupling, *J. Magn. Reson. A* 115 (2) (1995) 273–276.
- [44] Ē. Kupčē, R. Freeman, An adaptable nmr broadband decoupling scheme, *Chem. Phys. Lett.* 250 (5–6) (1996) 523–527.
- [45] Ē. Kupčē, R. Freeman, G. Wider, K. Wuthrich, Figure of merit and cycling sidebands in adiabatic decoupling, *J. Magn. Reson. A* 120 (2) (1996) 264–268.
- [46] Ē. Kupčē, R. Freeman, G. Wider, K. Wuthrich, Suppression of cycling sidebands using bi-level adiabatic decoupling, *J. Magn. Reson. A* 122 (1) (1996) 81–84.
- [47] Ē. Kupčē, R. Freeman, Compensation for spin–spin coupling effects during adiabatic pulses, *J. Magn. Reson.* 127 (1) (1997) 36–48.
- [48] R. Freeman, Ē. Kupčē, Decoupling: theory and practice. i. current methods and recent concepts, *NMR Biomed.* 10 (8) (1997) 372–380.
- [49] S. Cheatham, Spectral simplification of proton homonuclear correlation experiments utilizing ω_1 , ω_2 fluorine decoupling, *J. Fluorine Chem.* 140 (2012) 104–106.
- [50] N.S. Andersen, W. Kockenberger, A simple approach for phase-modulated single-scan 2d nmr spectroscopy, *Magn. Reson. Chem.* 43 (10) (2005) 795–797.
- [51] Y. Lin, A. Lupulescu, L. Frydman, Multidimensional j-driven nmr correlations by single-scan offset-encoded recoupling, *J. Magn. Reson.* 265 (2016) 33–44.
- [52] J.N. Dumez, L. Frydman, Multidimensional excitation pulses based on spatiotemporal encoding concepts, *J. Magn. Reson.* 226 (2013) 22–34.
- [53] J.N. Dumez, R. Schmidt, L. Frydman, Simultaneous spatial and spectral selectivity by spatiotemporal encoding, *Magn. Reson. Med.* 71 (2) (2014) 746–755.
- [54] J.-N. Dumez, Spatial encoding and spatial selection methods in high-resolution nmr spectroscopy, *Prog. Nucl. Magn. Reson. Spectrosc.* 109 (2018) 101–134.
- [55] G. Kervern, G. Pintacuda, L. Emsley, Fast adiabatic pulses for solid-state nmr of paramagnetic systems, *Chem. Phys. Lett.* 435 (1–3) (2007) 157–162.
- [56] N.M. Loening, B.J. van Rossum, H. Oschkinat, Broadband excitation pulses for high-field solid-state nuclear magnetic resonance spectroscopy, *Magn. Reson. Chem.* 50 (4) (2012) 284–288.
- [57] L.A. O’Dell, The worst kind of pulses in solid-state nmr, *Solid State Nucl. Magn. Reson.* 55–56 (2013) 28–41.
- [58] S. Wi, L. Frydman, An efficient, robust new scheme for establishing broadband homonuclear correlations in biomolecular solid state nmr, *ChemPhysChem* (2019).
- [59] I. Kaminker, S. Han, Amplification of dynamic nuclear polarization at 200 ghz by arbitrary pulse shaping of the electron spin saturation profile, *J. Phys. Chem. Lett.* 9 (11) (2018) 3110–3115.
- [60] T. Can, J. McKay, R. Weber, C. Yang, T. Dubroca, J. Van Tol, S. Hill, R. Griffin, Frequency-swept integrated and stretched solid effect dynamic nuclear polarization, *J. Phys. Chem. Lett.* 9 (12) (2018) 3187–3192.
- [61] F. Scott, E. Saliba, B. Albert, N. Alaniva, E. Sesti, C. Gao, N. Golota, E. Choi, A. Jagtap, J. Wittmann, M. Eckardt, W. Harneit, B. Corzilius, S.Th. Sigurdsson, A. Barnes, Frequency-agile gyrotron for electron decoupling and pulsed dynamic nuclear polarization, *J. Magn. Reson.* 289 (2018) 45–54.
- [62] C. Gao, N. Alaniva, E. Saliba, E. Sesti, P. Judge, F. Scott, T. Halbritter, S. Sigurdsson, A. Barnes, Frequency-chirped dynamic nuclear polarization with magic angle spinning using a frequency-agile gyrotron, *J. Magn. Reson.* 308 (2019) 106586.
- [63] J.J. Titman, A.L. Davis, E.D. Laue, J. Keeler, Selection of coherence transfer pathways using inhomogeneous adiabatic pulses - removal of zero-quantum coherence, *J. Magn. Reson.* 89 (1) (1990) 176–183.
- [64] M.J. Thrippleton, J. Keeler, Elimination of zero-quantum interference in two-dimensional nmr spectra, *Angew. Chem. Int. Ed.* 42 (33) (2003) 3938–3941.
- [65] M.J. Thrippleton, R.A.E. Edden, J. Keeler, Suppression of strong coupling artefacts in j-spectra, *J. Magn. Reson.* 174 (1) (2005) 97–109.
- [66] J. Forrer, S. Pfenninger, G. Sierra, G. Jeschke, A. Schweiger, B. Wagner, T. Weiland, Probeheads and instrumentation for pulse epr and endor spectroscopy with chirped radio frequency pulses and magnetic field steps, *Appl. Magn. Reson.* 10 (1–3) (1996) 263–279.
- [67] P.E. Spindler, Y. Zhang, B. Endewerd, N. Gershernzon, T.E. Skinner, S.J. Glaser, T.F. Prisner, Shaped optimal control pulses for increased excitation bandwidth in epr, *J. Magn. Reson.* 218 (2012) 49–58.
- [68] A. Doll, G. Jeschke, Fourier-transform electron spin resonance with bandwidth-compensated chirp pulses, *J. Magn. Reson.* 246 (2014) 18–26.
- [69] A. Doll, M. Qi, N. Wili, S. Pribitzer, A. Godt, G. Jeschke, Gd(iii)-gd(iii) distance measurements with chirp pump pulses, *J. Magn. Reson.* 259 (2015) 153–162.
- [70] G. Jeschke, S. Pribitzer, A. Doll, Coherence transfer by passage pulses in electron paramagnetic resonance spectroscopy, *J. Phys. Chem. B* 119 (43) (2015) 13570–13582.
- [71] P. Schops, P.E. Spindler, A. Marko, T.F. Prisner, Broadband spin echoes and broadband sifter in epr, *J. Magn. Reson.* 250 (2015) 55–62.
- [72] T.F. Segawa, A. Doll, S. Pribitzer, G. Jeschke, Copper eseeem and hyscore through ultra-wideband chirp epr spectroscopy, *J. Chem. Phys.* 143 (4) (2015) 044201.
- [73] A. Doll, G. Jeschke, Epr-correlated dipolar spectroscopy by q-band chirp sifter, *Phys. Chem. Chem. Phys.* 18 (33) (2016) 23111–23120.
- [74] K. Keller, A. Doll, M. Qi, A. Godt, G. Jeschke, M. Yulikov, Averaging of nuclear modulation artefacts in ridme experiments, *J. Magn. Reson.* 272 (2016) 108–113.
- [75] S. Pribitzer, A. Doll, G. Jeschke, Spidyan, a matlab library for simulating pulse epr experiments with arbitrary waveform excitation, *J. Magn. Reson.* 263 (2016) 45–54.
- [76] S. Pribitzer, T.F. Segawa, A. Doll, G. Jeschke, Transverse interference peaks in chirp ft-epr correlated three-pulse eseeem spectra, *J. Magn. Reson.* 272 (2016) 37–45.
- [77] A. Doll, G. Jeschke, Wideband frequency-swept excitation in pulsed epr spectroscopy, *J. Magn. Reson.* 280 (2017) 46–62.
- [78] S. Pribitzer, M. Sajid, M. Hülsmann, A. Godt, G. Jeschke, Pulsed triple electron resonance (trier) for dipolar correlation spectroscopy, *J. Magn. Reson.* 282 (2017) 119–128.
- [79] T. Bahrenberg, Y. Rosenski, R. Carmieli, K. Zibzener, M. Qi, V. Frydman, A. Godt, D. Goldfarb, A. Feintuch, Improved sensitivity for w-band gd(iii)-gd(iii) and nitroxide-nitroxide deer measurements with shaped pulses, *J. Magn. Reson.* 283 (2017) 1–13.
- [80] I. Kaminker, R. Barnes, S. Han, Arbitrary waveform modulated pulse epr at 200ghz, *J. Magn. Reson.* 279 (2017) 81–90.
- [81] A. Bieber, D. Bücker, M. Drescher, Light-induced dipolar spectroscopy – a quantitative comparison between lideer and laserimd, *J. Magn. Reson.* 296 (2018) 29–35.
- [82] N. Wili, G. Jeschke, Chirp echo fourier transform epr-detected nmr, *J. Magn. Reson.* 289 (2018) 26–34.
- [83] I. Ritsch, H. Hintz, G. Jeschke, A. Godt, M. Yulikov, Improving the accuracy of cu(ii)-nitroxide ridme in the presence of orientation correlation in water-

- soluble cu(ii)-nitroxide rulers, *Phys. Chem. Chem. Phys.* 21 (2019) 9810–9830.
- [84] L.A. O'Dell, R.W. Schurko, Qcpmg using adiabatic pulses for faster acquisition of ultra-wideline nmr spectra, *Chem. Phys. Lett.* 464 (1–3) (2008) 97–102.
- [85] I. Hung, Z. Gan, On the practical aspects of recording wideline qcpmg nmr spectra, *J. Magn. Reson.* 204 (2) (2010) 256–265.
- [86] L.B. Casabianca, D. Mohr, S. Mandal, Y.Q. Song, L. Frydman, Chirped cpmg for well-logging nmr applications, *J. Magn. Reson.* 242 (2014) 197–202.
- [87] L. Casabianca, Y. Sarda, E. Bergman, U. Nevo, L. Frydman, Single-sided stray-field nmr profiling using chirped radiofrequency pulses, *Appl. Magn. Reson.* 46 (8) (2015) 909–919.
- [88] J. Kuklinski, U. Gaubatz, F. Hioe, K. Bergmann, Adiabatic population transfer in a three-level system driven by delayed laser pulses, *Phys. Rev. A* 40 (11) (1989) 6741–6744.
- [89] U. Gaubatz, P. Rudecki, S. Schiemann, K. Bergmann, Population transfer between molecular vibrational levels by stimulated raman scattering with partially overlapping laser fields. a new concept and experimental results, *J. Chem. Phys.* 92 (9) (1990) 5363–5376.
- [90] J. Melinger, S. Gandhi, A. Hariharan, J. Tull, W. Warren, Generation of narrowband inversion with broadband laser pulses, *Phys. Rev. Lett.* 68 (13) (1992) 2000–2003.
- [91] B. Broers, H. Van Linden Van Heuvell, L. Noordam, Efficient population transfer in a three-level ladder system by frequency-swept ultrashort laser pulses, *Phys. Rev. Lett.* 69 (14) (1992) 2062–2065.
- [92] N. Vitanov, T. Halfmann, B. Shore, K. Bergmann, Laser-induced population transfer by adiabatic passage techniques, *Annu. Rev. Phys. Chem.* 52 (2001) 763–809.
- [93] A. Rangelov, N. Vitanov, L. Yatsenko, B. Shore, T. Halfmann, K. Bergmann, Stark-shift-chirped rapid-adiabatic-passage technique among three states, *Phys. Rev. A - Atomic, Mol., Opt. Phys.* 72 (5) (2005) 053403.
- [94] J. Randall, A.M. Lawrence, S.C. Webster, S. Weidt, N.V. Vitanov, W.K. Hensinger, Generation of high-fidelity quantum control methods for multilevel systems, *Phys. Rev. A* 98 (2018) 043414.
- [95] K. Zlatanov, N. Vitanov, Generation of arbitrary qubit states by adiabatic evolution split by a phase jump, *Phys. Rev. A* 101 (1) (2020) 013426.
- [96] I. Niemeyer, J.H. Shim, J. Zhang, D. Suter, T. Taniguchi, T. Teraji, H. Abe, S. Onoda, T. Yamamoto, T. Ohshima, J. Isoya, F. Jelezko, Broadband excitation by chirped pulses: application to single electron spins in diamond, *New J. Phys.* 15 (3) (2013) 033027.
- [97] J. Scheuer, I. Schwartz, Q. Chen, D. Schulze-Sünninghausen, P. Carl, P. Höfer, A. Retzker, H. Sumiya, J. Isoya, B. Luy, M.B. Plenio, B. Naydenov, F. Jelezko, Optically induced dynamic nuclear spin polarisation in diamond, *New J. Phys.* 18 (1) (2016) 013040.
- [98] A. Ajoy, R. Nazaryan, K. Liu, X. Lv, B. Safvati, G. Wang, E. Druga, J. Reimer, D. Suter, C. Ramanathan, C. Meriles, A. Pines, Enhanced dynamic nuclear polarization via swept microwave frequency combs, *Proc. Natl. Acad. Sci. U.S.A.* 115 (42) (2018) 10576–10581.
- [99] P. Zangara, S. Dhomkar, A. Ajoy, K. Liu, R. Nazaryan, D. Pagliero, D. Suter, J. Reimer, A. Pines, C. Meriles, Dynamics of frequency-swept nuclear spin optical pumping in powdered diamond at low magnetic fields, *Proc. Natl. Acad. Sci. U.S.A.* 116 (7) (2019) 2512–2520.
- [100] J. Dormand, P. Prince, A family of embedded runge-kutta formulae, *J. Comput. Appl. Math.* 6 (1) (1980) 19–26.
- [101] I. Kuprov, Fokker-planck formalism in magnetic resonance simulations, *J. Magn. Reson.* 270 (2016) 124–135.
- [102] A.J. Allami, M.G. Concilio, P. Lally, I. Kuprov, Quantum mechanical mri simulations: Solving the matrix dimension problem, *Sci. Adv.* 5 (7) (2019).
- [103] H. Hogben, M. Krzyszynia, G. Charnock, P. Hore, I. Kuprov, Spinach – a software library for simulation of spin dynamics in large spin systems, *J. Magn. Reson.* 208 (2) (2011) 179–194.
- [104] N.A. Sinitsyn, V.Y. Chernyak, The quest for solvable multistate landau-zener models, *J. Phys. A* 50 (25) (2017) 255203.
- [105] N.A. Sinitsyn, E.A. Yuzbashyan, V.Y. Chernyak, A. Patra, C. Sun, Integrable time-dependent quantum hamiltonians, *Phys. Rev. Lett.* 120 (2018) 190402.
- [106] P.-L. Giscard, K. Lui, S.J. Thwaite, D. Jakusch, An exact formulation of the time-ordered exponential using path-sums, *J. Math. Phys.* 56 (2015) 053503.
- [107] F.T. Hioe, Solution of bloch equations involving amplitude and frequency modulations, *Phys. Rev. A* 30 (4) (1984) 2100–2103.
- [108] J. Zhang, M. Garwood, J.Y. Park, Full analytical solution of the bloch equation when using a hyperbolic-secant driving function, *Magn. Reson. Med.* 77 (4) (2017) 1630–1638.
- [109] J.M. Böhlen, G. Bodenhausen, Experimental aspects of chirp nmr-spectroscopy, *J. Magn. Reson. A* 102 (3) (1993) 293–301.
- [110] S. Meister, J.T. Stockburger, R. Schmidt, J. Ankerhold, Optimal control theory with arbitrary superpositions of waveforms, *J. Phys. A* 47 (49) (2014) 495002.
- [111] D.L. Goodwin, W.K. Myers, C.R. Timmel, I. Kuprov, Feedback control optimisation of esr experiments, *J. Magn. Reson.* 297 (2018) 9–16.
- [112] J. Wei, E. Norman, Lie algebraic solution of linear differential equations, *J. Math. Phys.* 4 (1963) 575–581.
- [113] J. Wei, E. Norman, On global representations of the solutions of linear differential equations as a product of exponentials, *Proc. Am. Math. Soc.* 15 (1964) 327.
- [114] G. Campolieti, B.C. Sanctuary, The wei–norman lie-algebraic technique applied to field modulation in nuclear magnetic resonance, *J. Chem. Phys.* 91 (1989) 2108–2123.
- [115] J. Zhou, C. Ye, Rotation-operator approach and spin dynamics in a time-varying magnetic field, *Phys. Rev. A* 50 (1994) 1903–1905.
- [116] M. Foroozandeh, R.W. Adams, N.J. Meharry, D. Jeannerat, M. Nilsson, G.A. Morris, Ultrahigh-resolution nmr spectroscopy, *Angew. Chem. Int. Ed. Engl.* 53 (2014) 6990–6992.
- [117] M. Foroozandeh, R.W. Adams, M. Nilsson, G.A. Morris, Ultrahigh-resolution total correlation nmr spectroscopy, *J. Am. Chem. Soc.* 136 (2014) 11867–11869.
- [118] M. Foroozandeh, R.W. Adams, P. Kiraly, M. Nilsson, G.A. Morris, Measuring couplings in crowded nmr spectra: pure shift nmr with multiplet analysis, *Chem. Commun.* 51 (2015) 15410–15413.
- [119] M. Foroozandeh, L. Castañar, L.G. Martins, D. Sinnaeve, G.D. Poggetto, C.F. Tormena, R.W. Adams, G.A. Morris, M. Nilsson, Ultrahigh-resolution diffusion-ordered spectroscopy, *Angew. Chem. Int. Ed. Engl.* 55 (2016) 15579–15582.
- [120] M. Foroozandeh, G.A. Morris, M. Nilsson, Psyche pure shift nmr spectroscopy, *Chem.: Eur. J.* 24 (2018) 13988–14000.